The Dwarf Spheroidal Companions to M31: WFPC2 Observations of Andromeda II[1] [2]

G. S. Da Costa

Research School of Astronomy & Astrophysics, Institute of Advanced Studies, The Australian National University, Private Bag, Weston Creek Post Office, ACT 2611, Australia

Electronic mail: gdc@mso.anu.edu.au

T. E. Armandroff

Kitt Peak National Observatory, National Optical Astronomy Observatories, P.O. Box 26732, Tucson, Arizona 85726

Electronic mail: armand@noao.edu

Nelson Caldwell

F. L. Whipple Observatory, Smithsonian Institution, P.O. Box 97, Amado, Arizona 85645

Electronic mail: caldwell@flwo99.sao.arizona.edu

and

Patrick Seitzer

Department of Astronomy, University of Michigan, Ann Arbor, Michigan 48109

Electronic mail: seitzer@astro.lsa.umich.edu

---

[1]Based on observations with the NASA/ESA *Hubble Space Telescope*, obtained at the Space Telescope Science Institute, which is operated by the Association of Universities for Research in Astronomy, Inc., (AURA), under NASA Contract NAS 5-26555.

[2]Based, in part, on observations obtained at Kitt Peak National Observatory, a division of the National Optical Astronomy Observatories, which is operated by AURA Inc. under cooperative agreement with the National Science Foundation.

Received _____; accepted _____

Accepted for publication in the February 2000 issue of the Astronomical Journal

ABSTRACT

The *Hubble Space Telescope* WFPC2 camera has been used to image Andromeda II, a dwarf spheroidal (dSph) companion to M31. The resulting color-magnitude (c-m) diagrams reveal the morphology of the horizontal branch (HB) in this dwarf galaxy. We find that like Andromeda I, and like most of the Galactic dSph companions, the HB morphology of And II is predominantly red. Unlike And I, however, there is no evidence for a radial gradient in HB morphology in the And II data. Based on a comparison with a combination of standard Galactic globular cluster c-m diagrams scaled to reproduce the And II mean abundance and abundance dispersion, we interpret the observed HB morphology of And II as indicating that at least 50% of the total stellar population is younger than the age of the globular clusters. This inference is strengthened by the small number of confirmed upper-AGB carbon stars in And II. The relatively faint luminosities ($M_{bol} \approx$ –4.1) of these stars, however, suggest an age or ages nearer 6–9 Gyr, rather than 1–3 Gyr, for this population. On the other hand, the existence of blue HB and RR Lyrae variable stars in And II argues for the existence of an additional old (age $>$ 10 Gyr) population in this dSph. Thus And II has had an extended epoch of star formation like many of the Galactic dSphs. The mean magnitude of the blue HB in And II suggests $(m–M)_0 = 24.17 \pm 0.06$ and that And II is 125 $\pm$ 60 kpc closer than M31 along the line-of-sight. This confirms the association of And II with M31, rather than with M33 to which And II lies closer on the sky. The true distance of And II from the center of M31 is between ∼160 and ∼230 kpc, comparable to the Galactocentric distances of Fornax and of the Leo dSphs. With the current samples of dSph companions, the size of the Galaxy's and M31's dSph satellite systems are comparable, with outer radii of order 250 kpc. The And II

red giant branch colors yield a mean abundance of <[Fe/H]> = –1.49 ± 0.11 and a surprisingly large internal abundance spread, which can be characterised by σ_{int}([Fe/H]) ≈ 0.36 dex. Both these values are in good agreement with the recent ground-based spectroscopic study of Côté *et al.* [1999, AJ, 118, 1645]. The And II abundance dispersion found here is considerably larger than that derived for And I from an identical analysis of similar data (σ_{int}([Fe/H]) = 0.21 dex). Thus despite having very similar luminosities and mean metal abundances, these two M31 dSph companions have clearly had different chemical evolution histories. We find that we cannot model the abundance distribution in And II with single component simple chemical enrichment models. However, we can reproduce the form of the distribution if we assume two components, each with a simple model abundance distribution. The "metal-poor" component has mean abundance $\log(< z >/z_{sun})$ = –1.6, while the "metal-rich" one has mean abundance $\log(< z >/z_{sun})$ = –0.95 and is outnumbered by the metal-poor population by a ratio of ∼2.3 to 1. We end by concluding that the diversity of evolutionary histories evident among the Galactic dSph companions is now also firmly established among the dSph satellites of M31. An Appendix discusses minor revisions to our earlier And I results that arise from the calibration and analysis techniques adopted in this paper. In particular, our comparisons with ground-based photometry indicate that the zeropoint for the WFPC2 $F450W$ to B transformation should be modified, by 0.055 mag, to produce fainter B magnitudes and thus redder $B - V$ colors.

Subject headings: galaxies: dwarf — galaxies: individual (Andromeda I, Andromeda II) — galaxies: photometry — galaxies: stellar content — galaxies: abundances — Local Group

1. Introduction

The first Galactic dwarf spheroidal (dSph) companion galaxy, Sculptor, was discovered in 1938 by Harlow Shapley (Shapley 1938). Shortly afterwards Baade & Hubble (1939) reported that the Sculptor system contained (globular) cluster-type short period variables, large numbers of "ordinary giants", and that amongst the brighter Sculptor stars, extremely blue or extremely red stars were lacking. Thus began the study of the stellar populations of dSph galaxies.

By the 1990s the Galaxy was known to have nine dSph companions whose stellar populations have been studied in considerable detail, using both ground-based and *Hubble Space Telescope* (HST) observations. Undoubtedly, the most unexpected result of these studies is the fascinating diversity of star formation histories they have revealed (see, for example, recent reviews by Da Costa 1998 and Grebel 1999). The Galactic dSph galaxies have stellar populations that range from purely or predominantly old (e.g. Ursa Minor) through systems such as Leo I, in which the bulk of the population has ages between 1 and 7 Gyr (Gallart *et al.* 1999a, b). While there is some indication of a correlation between intermediate-age population fraction and Galactocentric distance (e.g. van den Bergh 1994), which hints at the influence of the "parent" galaxy on the evolution of the dSph satellites, we have at this moment in time little understanding of what lies behind this diversity of star formation histories.

One way to improve our knowledge of the origin of this diversity is to study the dSph satellite systems around other galaxies. The dSph companions to M31, which after the recent discoveries of Armandroff *et al.* (1998), Armandroff *et al.* (1999) and Karachentsev & Karachentseva (1999) now number six in total, provide the nearest examples of this class of galaxy beyond the Milky Way. From the ground, studies of these M31 dSph systems are limited to the upper $\sim$2 mags of the red giant branch. With the WFPC2 camera aboard

HST, however, photometry can be obtained for significantly fainter stars while at the same time the accuracy for the brighter stars can be considerably improved. Indeed with HST/WFPC2 it is possible to reach sufficiently faint that color-magnitude (c-m) diagrams can be produced which reveal the morphology of the horizontal branch in these systems. When coupled with the mean abundance and intrinsic abundance spread, the horizontal branch morphology can then yield important information on the star formation history. Further, the HST/WFPC2 photometry, because of the significantly reduced effects of image crowding, allows a much better determination of the giant branch intrinsic width. This in turn can provide important information on the chemical enrichment processes that took place. Finally, the WFPC2 photometry can also be used to place limits on the age of, or even detect, the youngest main sequence population present.

In Da Costa *et al.* (1996, hereafter Paper I) we presented WFPC2 photometry for the M31 dSph companion And I, and showed, *inter alia*, that this dSph has a dominant red horizontal branch morphology like most of the Galaxy's dSph companions. The results were interpreted as indicating that the bulk of And I's stellar population was $\sim$10 Gyr old. The presence of blue horizontal branch and RR Lyrae stars, however, testified to the presence of an older population in And I. Thus, like most of the Galactic dSph companions, And I has had an extended epoch of star formation. The WFPC2 data also revealed a radial gradient in And I's horizontal branch (HB) morphology, in the sense that there are relatively more blue HB stars beyond the dSph's core radius. This was interpreted as evidence that the subsequent star formation was more centrally concentrated than the initial episode. In this paper we concentrate on And II. Observations of And III with WFPC2 were obtained recently and they will be the subject of the next paper in this series. The newly discovered systems And V and And VI are scheduled to be observed in a Cycle 8 HST General Observer program.

And II is one of the more luminous M31 dSph companions and, aside from And III, it has the largest apparent flattening of these systems (Caldwell *et al.* 1992, Caldwell 1999). It lies ∼140 kpc in projection from the center of M31 in the direction of M33. Indeed, pending the results presented in this paper, it is possible that And II is associated with M33 rather than M31. And II is unique among the M31 dSph satellites in that it is the only one in which the existence of upper-AGB carbon stars has been spectroscopically confirmed (Aaronson *et al.* 1985, see also Côté *et al.* 1999b). These stars are relatively common in the Galactic dSphs and are an indicator of the presence of an intermediate-age (∼1 – 10 Gyr) population. Previous ground-based studies of And II include that of König *et al.* (1993) in which it was suggested that And II was somewhat closer along the line-of-sight than M31, and that this dSph perhaps has a relatively large intrinsic metallicity spread. Our WFPC2 data allow a more precise and quantitative evaluation of these possibilities. Côté *et al.* (1999b) have also investigated the mean metallicity and intrinsic metallicity spread using (ground-based) low resolution spectra of a sample of And II red giants.

The remainder of this paper is split into three sections. In Sect. 2 we discuss the observations, the photometric techniques employed and the calibration process adopted. In Sect. 3, the WFPC2 c-m diagrams are presented and main results of the paper discussed. These include the HB morphology, the true distance of And II from the center of M31, the mean abundance and abundance dispersion, and inferences on the age(s) of the stellar population. The consequences of our results in the wider context of dSph evolution are discussed in the final section. An Appendix describes minor revisions to the And I results of Paper I made necessary by the reduction and analysis techniques adopted in this paper.

2. Observations and Reductions

Andromeda II was imaged with the WFPC2 instrument aboard the *Hubble Space Telescope* on 1997 August 29 and again, at the same orientation, on 1997 September 3 as per our GO Program 6514. The first set of observations consisted of three 1200 s integrations through the $F555W$ ("Wide-V") filter and seven 1300 s integrations through the $F450W$ ("Wide-B") filter. The second set of observations used identical exposure times but there were four $F555W$ and eight $F450W$ integrations. The field of And II contains a number of bright foreground stars (e.g. Caldwell *et al.* 1992, Fig. 2). Consequently, to avoid any possible deleterious effects from these stars, a WFALL-FIX center offset from the center of the dSph, and a range of allowable orientations, was specified at the Phase-II stage. The actual observations placed the center of And II approximately on the boundary between the WF3 and WF4 chips $\sim 70''$ from the WFPC2 pyramid apex. The second set of observations was displaced from this center by a small amount, nominally 9.5 WF pixels in both x and y. This facilitates distinguishing real stars from instrumental defects, such as hot pixels, and allows an assessment of the errors in the photometry. In this respect these And II observations are similar to those of And I described in Paper I. The location of the section of And II imaged with WFPC2, relative to the full extent of this dSph galaxy, is shown in Fig. 1.

The raw frames were processed via standard STScI pipeline procedures. In particular, the DARKCORR (dark correction) frame used, which includes the (time variable) hot pixels, was obtained just 4 days before the first set of observations. The processed frames were then separated into the images for each individual CCD, multiplied by the appropriate geometric distortion image as supplied by STScI, and trimmed of the vignetted regions using the boundaries recommended in the WFPC2 Handbook. The locations of bright stars were then measured on each set (one for each combination of filter, position and CCD) to

ascertain whether there were any systematic changes in position during the sequence of observations. None were found. The individual images for each set were then combined using the *gcombine* task within the STSDAS package. This task removes cosmic rays through a sigma-rejection criterion but one must be careful that the centers of bright stars are not adversely affected at the same time. We experimented with the parameter *snoise* until we found values (typically $\sim$0.10) that gave excellent cosmic ray rejection but for which magnitudes of bright stars on the combined frame were not significantly different ($\lesssim$0.01 mag) from the average of the values from the individual frames. A mosaic made from the combination of four 1200 s $F555W$ frames is shown in Fig. 2. As for the And I data in Paper I, the HST/WFPC2 combination completely resolves this dSph; indeed the And II stars are relatively uncrowded. There is also no indication of any star clusters on this image (nor are there any candidates from ground-based imaging), a result that is not surprising given that And II is $\sim$2 magnitudes fainter than the least luminous dSph galaxy with an identified star cluster population.

2.1. Photometry

The relatively uncrowded nature of the And II frames means that we can employ the techniques of aperture photometry. We note first, however, that because of the small number of stars on the PC1 frames ($\sim$5% of the total number on the WF chips), and because of the lack of "bright" stars with which to determine the PC1 aperture corrections, we have decided not to use the PC1 data. All subsequent discussion then applies solely to the three WF CCDs. Briefly, the *daofind* routine within IRAF/DAOPHOT was used to generate an image-center coordinate list for each of the 12 combinations of filter, position and WF frame. Aperture photometry using a 2 pixel radius aperture was then carried out for the objects on the input lists, with the "sky" taken as the mode of the pixel values in

an annulus of inner radius 5 and outer radius 15 pixels. This was then followed by the determination of the aperture corrections – the difference between the 2 pixel measurement aperture and the 5 pixel standard aperture adopted by Holtzman *et al.* (1995b, hereafter H95). Typically a dozen or so of the brightest, most isolated stars spread across each WF image were used. The aperture corrections for the individual stars, which showed a standard deviation of typically 0.02 mag, were then averaged to form a single correction for each filter/position/frame combination. The corrected photometry lists for the two positions and a given filter were then compared. There were no indications of any systematic differences and as a result, a single magnitude was generated by averaging the two measurements. Stars detected on only one frame were discarded. Similarly, the combined photometry lists for the $F555W$ and $F450W$ filters were matched to produce $F450W - F555W$ colors. Again stars not detected in both filters were ignored. While this does limit the data to those stars detected on the "shallowest" frames (the 3×1200 s $F555W$ combination for bluer stars and the 7×1300 s $F450W$ combination for redder stars) it does ensure that the objects in the photometry lists are real. At this stage corrections for exposure time, gain factors and zeropoint were also applied to place the photometry on the H95 system.

Although the frames are relatively uncrowded, there are still occasions where the signal in the measurement aperture for a star is contaminated by signal from a nearby companion, leading to an (undetected) error in the measured magnitude and to an increase in the scatter in the c-m diagram. To avoid this possibility, we have removed from the photometry lists any star whose center lay within 5 pixels of the center of another star. This reduced the sample by less than 10% but reduced the scatter in the c-m diagram. Finally, the remaining "stars" were visually inspected on the four-exposure-combined $F555W$ images and a small number of objects, mostly marginally resolved galaxies, removed. In these respects the procedures followed here are identical to those used for And I in Paper I. The final And II sample then consists of 1765 stars from the three WF frames.

2.1.1. Charge-Transfer Efficiency Corrections

The WFPC2 CCDs are known (e.g. Holtzman *et al.* 1995a) to suffer from poor charge-transfer efficiency (CTE) which can affect photometry obtained from WFPC2 images, especially for faint stars on exposures with a low background (sky) level. Stetson (1998) gives an excellent description of the likely physical processes involved. Holtzman *et al.* (1995a) proposed for low background situations, as in our exposures where the sky level is typically $\sim$65 e^-pixel^{-1} for $F555W$ and $\sim$30 e^-pixel^{-1} for $F450W$, that the effect of the poor CTE could be reduced by imposing a 0.04 mag/800 pixel ramp correction, in the sense that stars with higher y coordinate become relatively brighter. This correction process was adopted in Paper I. More recently, however, Whitmore & Heyer (1997, hereafter WH97), and subsequently Stetson (1998), have investigated the CTE effects in greater detail. Both report that the CTE effects are a function of not only the y, but also the x, coordinate on the frames. WH97 give a variety of formulae to correct for the effects. We applied their equations 2c and 3c (2 pixel radius aperture, local sky) to first correct the individual 2 pixel aperture magnitudes on all the filter/position/WF frame photometry lists. We then used WH97 equations 2d and 3d (5 pixel radius aperture, local sky) to correct the magnitudes of the aperture correction stars and thus generate new aperture corrections. We then regenerated the final averaged, crowding corrected, edited and calibrated photometry list. For our data, the WH97 CTE correction process makes a typical And II red horizontal branch star near the center of a WF frame brighter by $\sim$0.04 mag and bluer by $\sim$0.01 mag relative to the uncorrected photometry; the effects are about twice as large for stars that have large x and y coordinates. Stetson (1998) indicates that his formalism generally results in similar corrections to those of WH97, so we have chosen not to investigate the application of Stetson's formalism to our data.

2.1.2. Photometric Errors

With the CTE corrected data set we can now investigate the photometric errors, i.e. the errors that arise from the measurement process, as distinct from systematic errors that can come from uncertainty in the aperture corrections, in the zeropoint calibration, in the CTE correction process and so on. To do this we return to the photometry lists for the two separate pointings and compare colors and magnitudes for those stars in the final sample. The results of this process are presented in Table 1. It lists, for the specified magnitude bins, the average error in the mean of the two measures (either magnitude or color). As was found in Paper I, at fainter magnitudes for these uncrowded stars, the photometric errors are essentially those expected on the basis of photon statistics errors alone. The errors themselves though are somewhat larger than in Paper I as a consequence of the shorter total integration times. At brighter magnitudes, however, the photometric errors approach a lower limit of $\sim$0.015 mag, again as was found in Paper I. We ascribe this limit on the photometric precision to the effects of flat fielding and dark subtraction, and to the individual frame combination process adopted. The existence of this limit, however, does not affect the interpretation of the data in any way.

In the comparison process a small number of stars were identified as having $F555W$, $F450W$ or $F450W - F555W$ differences larger by 3.5σ or more, than the mean difference for their magnitude (which was always close to zero). As we shall see in Sec. 3.1.2, the majority of these stars are likely to be And II RR Lyrae variable stars. Fig. 3 then shows the color-magnitude diagram for the final And II sample on the HST/WFPC2 photometric system of H95. The 54 candidate variable stars are plotted with a different symbol.

2.1.3. V, $B-V$ Zeropoint Calibration

In paper I we adopted the $F555W$ to V and $F450W$ to B transformations as given in H95. For $F555W$ the transformation is derived from ground-based observations using a replica of the flight system (see H95 for details) but for $F450W$ the transformation is not directly determined. Instead it comes from the convolution of the HST+WFPC2+CCD+$F450W$ filter response curve with a library of stellar spectra. It is then (perhaps) less well determined than that for $F555W$. In order to investigate these transformations, or more particularly their zeropoints, we obtained a set of deep B and V images of And II with the WIYN[3] 3.5 m telescope via the NOAO WIYN Queue process. These images were taken in excellent seeing (FWHM $\approx 0.55''$) and under photometric conditions. A number of photometric standard star fields were also observed to provide calibration. These photometric standard observations generated very well determined transformations from the WIYN instrumental system to the B, V standard system. We then inspected the WFPC2 and WIYN images and selected $\sim$40 stars distributed over the WF frames that could be reliably measured on the WIYN images. By necessity, these stars are all at or near the top of the And II red giant branch. The differences between the WFPC2 and the WIYN photometry for these stars were then derived. Considering first the comparison of V_{WFPC2}, which arises from the CTE corrected $F555W$ photometry, and V_{WIYN}, we find no indication of any offset, nor any trend with magnitude or color. For the 41 stars involved in this comparison, the mean value of $V_{WFPC2} - V_{WIYN}$ is 0.007 mag with a standard error in this mean of 0.010 mag. We conclude, as have many others, that the $F555W$ to V transformation is well determined. The situation for $F450W$ and B, however, is not as good. As illustrated in Fig. 4 we find that there is a clear offset between

[3]The WIYN Observatory is a joint facility of the University of Wisconsin-Madison, Indiana University, Yale University and the National Optical Astronomy Observatories.

B_{WFPC2}, which arises from the CTE corrected $F450W$ photometry and the H95 synthetic transformation, and B_{WIYN}. The mean value of $B_{WFPC2} - B_{WIYN}$ is –0.053 mag with a standard error in this mean of 0.010 mag. There does not seem to be any indication that this offset varies with color, though the range available is limited ($1.0 \lesssim B - V \lesssim 1.7$).

To confirm this apparent zeropoint offset, we searched the HST archive for additional observations which employed the $F450W$ filter and which targeted objects with established B, V photometry. The WFPC2 Cycle 6 Calibration Program 6935 proved ideal for this test, since it contains $F450W$ and $F555W$ observations of the ω Cen standard star field. Ground-based B, V photometry is available for this field from Walker (1994). We performed photometry on the WFPC2 frames of the ω Cen standard star field in exactly the same way as was done for And II, including the application of the WH97 CTE corrections. This led to 42 measures of 20 standards obtained from three different WFPC2 data sets (different orientations meant that not all stars are found on all frames). The magnitudes and colors for the multiply observed stars were averaged and the WFPC2 data for all compared with the Walker (1994) ground-based values. Once again we find no strong evidence for any systematic differences when comparing V_{WFPC2} with V_{Walker}. For the $B - V$ colors, however, an offset almost identical in size to that found for And II is present. Weighting by the number of observations, the mean value of $(B-V)_{WFPC2} - (B-V)_{Walker}$ is –0.049 mag with a standard error in the mean of 0.006 mag, for 38 observations of 18 stars (we have excluded the three observations of the sole blue star and one notably discrepant measure). The majority of the stars in this comparison are ω Cen main sequence stars and are thus bluer in color than the And II red giants. Yet, as for And II, there is no evidence for any correlation between the difference $(B - V)_{WFPC2} - (B - V)_{Walker}$ and $(B - V)_{Walker}$, at least for $(B - V)$ colors redder than $(B - V) \approx 0.50$ (the reddest star in the ω Cen sample has $B - V = 1.33$ and thus there is color overlap with the And II sample). As to whether this offset applies for bluer colors, we lack sufficient information to be certain one way or

the other. We assume that it does but, fortunately, no results in this paper are affected by this latter assumption.

Thus, in transforming the And II $F450W$, $F555W$ CTE corrected photometry to the standard B,V system, we have adopted a zeropoint shift of 0.055 mag relative to the H95 relation, in the sense of fainter B magnitudes and thus redder $B-V$ colors. The resulting c-m diagram, without the candidate variables, is shown in Fig. 5. The implications of this change in adopted $B-V$ zeropoint, and of the WH97 CTE corrections, for the And I results presented in Paper I are discussed in Appendix A.

3. Results

3.1. The Color-Magnitude Diagrams of And II

In general, the c-m diagrams for And II presented in Figs. 3 and 5 bear a strong resemblance to those for And I in Paper I (and in Appendix A). The basic morphology is that of an old stellar population – there is a red giant branch with a notable color width, especially at brighter magnitudes, and a horizontal branch showing a large color range but with a predominance of red horizontal branch stars. A population of stars fainter than the horizontal branch and bluer than the giant branch is also evident. The most conspicuous difference between the And I and And II c-m diagrams, however, is the relative lack of objects redder than the "red edge of the giant branch" in the And II c-m diagram. In Paper I we argued that such stars in the And I c-m diagram were predominantly red giants from the halo of M31; red Galactic foreground stars were approximately a factor of two less important. That assertion in Paper I is supported here – since And II lies $\sim$3 times further in projection from the center of M31 than does And I, we expect the And II c-m diagram to be much less contaminated by M31 halo stars, and this is what we see. Indeed, using

the predictions of Ratnatunga & Bahcall (1985) as a guide, we can suggest that the small number of redder objects in Figs. 3 and 5 are probably all Galactic foreground objects[4]. Consequently, given that the color distribution of Galactic foreground objects greatly favors red stars at these magnitudes (e.g. Ratnatunga & Bahcall 1985), we conclude that the degree of contamination of the And II c-m diagrams by non-member objects is negligible.

3.1.1. The Horizontal Branch Morphology

It is clear from Figs. 3 and 5 that the morphology of the horizontal branch in And II is dominated by red stars. As was the case for And I, the red side of the And II HB is superposed on the red giant branch and there is no clear distinction between the red giants and the core helium burning stars at this luminosity. In Paper I we noted that this is a consequence of three effects: a spread in the colors of HB and red giant stars of similar luminosity due to photometric errors in $F450W - F555W$; the lower sensitivity (relative to $B - V$) of $F450W - F555W$ to differences in effective temperature; and the presence (see Sect. 3.4) of a significant metal abundance spread, which results in horizontal branch stars from the more metal-rich population having comparable colors to similar luminosity red giants from the metal-poor population. These effects are no doubt also responsible for the appearance of Figs. 3 and 5 at HB luminosities.

To quantify the And II HB morphology we follow Paper I and calculate the HB morphology index $i = b/(b + r)$, where b and r are the number of blue and red HB stars, respectively. In particular, we take r as the number of stars with $24.65 \leq F555W \leq 25.15$

[4]One definite exception to this statement is the star that lies ∼0.4 mag fainter but at the same color as the brightest, reddest giants in Figs. 3 and 5. This is Côté *et al.* (1999b) star 3; a spectroscopically identified carbon star that is a highly probable And II member.

and $0.35 \leq F450W - F555W \leq 0.60$. The red limit was fixed by noting that a color histogram for stars in this magnitude range shows a decline redward of this color, and thus it represents a reasonable estimate for the color limit beyond which red giants outnumber red HB stars. The same limit was adopted in Paper I. For b, we count the stars with $24.65 \leq F555W \leq 25.60$ and $-0.35 \leq F450W - F555W \leq 0.25$, less the small number of stars with $25.15 \leq F555W \leq 25.60$ and $0.10 \leq F450W - F555W \leq 0.25$ since they are probably not blue HB stars. Including the candidate variables, we find $r = 343$ and $b = 76$ for $i = 0.18 \pm 0.02$, where the error is calculated assuming that b and r follow Poisson statistics. If we exclude the candidate variables, then the value of i, 0.17 ± 0.02, is essentially unchanged.

For And I we found $i = 0.13 \pm 0.01$ suggesting that the And II HB morphology is somewhat bluer than that of And I. In quantitative terms, if And II had possessed the same HB morphology index as And I, then for the same total number of HB stars as observed we would have expected ∼50 blue HB stars. In fact approximately 50% more than this are present. This result does not depend on the adopted red limit for defining the red HB population. If instead of $F450W - F555W = 0.60$, we adopt 0.52 for this limit, the absolute values of the morphology index i change but the result that And II contains ∼50% more blue HB stars relative to And I, remains.

Despite this difference though, the And II HB morphology, like that of And I, is dominated by red HB stars. Standard Galactic globular clusters whose abundances encompass the And II mean (<[Fe/H]> ≈ –1.5, see Sect. 3.3) have horizontal branch morphologies that show an even, or a blueward biased, distribution of HB stars. For example, using the R and B numbers given in Lee *et al.* (1994), we find $i = 0.74 \pm 0.04$ for M5 ([Fe/H] = –1.40) and $i = 0.45 \pm 0.05$ for M4 ([Fe/H] = –1.28) while the clusters NGC 6752 ([Fe/H] = –1.54) and M13 ([Fe/H] = –1.65) have $i = 1.00$, i.e. entirely blue HB morphologies. At first sight this difference between the value of $i = 0.18 \pm 0.02$ for And II

and those for these standard Galactic globular clusters, suggests that And II should be classified as showing the *second parameter effect* in the same way as does And I (Paper I). For instance, the well known "second parameter" Galactic globular cluster NGC 362 ([Fe/H] = –1.28) has a dominant red HB morphology characterized by $i = 0.04 \pm 0.02$, while NGC 7006 ([Fe/H] = –1.59), also a second parameter cluster, has $i = 0.23 \pm 0.06$. However, the large abundance range in And II (see Sect. 3.4) means that any conclusion regarding the second parameter nature of And II that is based solely on these simple comparisons must be viewed with some caution. Nevertheless, we shall show in Sect. 3.5 that the HB morphology of And II cannot be modelled with a combination of standard (i.e. non second parameter) Galactic globular cluster horizontal branches – a significant second parameter component to the HB morphology is required. Thus we are entitled to claim that And II is a second parameter object along with And I and most of the Galactic dSph companions.

One of the most intriguing results of Paper I was the discovery that And I shows a radial gradient in its HB morphology, in the sense that there are relatively more blue HB stars outside the dSph's core radius. Similar HB morphology gradients also exist in at least two Galactic dSphs but are absent in others (Paper I). Consequently, we have used our data to investigate whether or not such a HB morphology gradient is present in And II. According to Caldwell *et al.* (1992), And II has an ellipticity of 0.3 and a (geometric mean) core radius of $\sim$100″ ($\sim$120″ on the major axis). We first split our And II photometry sample into inside and outside the core radius samples, using the appropriate elliptical boundary (the position angle of the major axis for And II is $\sim$155°). The average radial distances of the stars in these samples are 58″ and 130″, respectively, with the most distant stars $\sim$170″ from the center. We also split the sample, again along an elliptical boundary, into two groups with approximately equal numbers of stars. This occurs for a major axis radius of $\sim$75″ or $\sim 0.6 r_{core}$. The average radial distances for these samples are 42″ and 99″, respectively.

We find, using the sample which includes the candidate variable stars, that inside the core radius $i = 0.18 \pm 0.02$ (r=289, b=62) while outside the core $i = 0.21 \pm 0.05$ (54, 14). Similarly, inside the ∼50% sample radius, $i = 0.16 \pm 0.03$ (180, 35) while outside this radius $i = 0.20 \pm 0.03$ (163, 41). None of these differences are statistically significant (recall from Paper I that the value of i for And I changed from $i = 0.11 \pm 0.01$ inside the core radius to $i = 0.20 \pm 0.03$ outside it, a 2.9σ difference). We conclude then that And II apparently differs from And I in that it lacks any significant HB morphology radial gradient, at least within ∼1.3 core radii. The existence of this difference should not be seen as too surprising since, as we noted in Paper I, among the Galactic dSphs Leo II and Sculptor possess similar HB morphology gradients to And I but Carina does not.

3.1.2. RR Lyrae Variables

In Fig. 3 there are approximately 30 candidate variable stars with magnitudes similar to that of the horizontal branch. These stars are most likely to be RR Lyrae variables in And II. To investigate this assertion we have performed aperture photometry for a subset of these candidates in the same way as discussed above, except using the individual WFPC2 frames rather than the combinations. This process yields, cosmic-ray contamination willing, a maximum of 7 individual $F555W$ and 15 $F450W$ magnitudes for each candidate. A plot of these magnitudes against the mid-exposure Julian date then clearly indicates whether or not the candidate varies in a systematic way. Of the 13 candidates investigated in this fashion, all showed clear evidence of variability with timescales and amplitudes typical for RR Lyrae stars. Attempts were then made to find periods for these stars. However, the relatively short duration of the two sets of observations, ∼0.2 d, compared to the interval between them, ∼4.7 d, often meant that it was difficult to choose between two distinct periods which gave similar light curves (typically resulting from the ambiguity as

to whether there were 8 or 9 cycles between the two sets of observations). The $F555W$ observations were frequently used (along with the assumption of ∼constant color) to reduce this ambiguity as was the assumption that these RR Lyraes should follow an approximate period-amplitude relation. Nevertheless, it was often not possible to determine a unique period. Typical light curves resulting from this process are shown in Fig. 6. These light curves, and others not shown, identify most of these stars as Type-ab RR Lyraes. For one star it was not possible to generate a reasonable light curve while another may be a Type-c variable with a lower amplitude and shorter period.

In this process it was noticed that two of the five HB stars with extremely blue $F450W - F555W$ colors in Fig. 3 are RR Lyrae variables, while the other three such stars were not flagged as variable candidates. Consequently, these three stars were also investigated for variability in the same way as the other candidates. Perhaps not surprisingly, they were also found to be RR Lyrae variables. This demonstrates that the method of identifying variables from significant differences in the mean magnitudes or colors between the two data sets, while successful, is not likely to generate a complete set of variables. A full investigation of the frequency of RR Lyrae variables on the And II horizontal branch, and a discussion of the nature of the non-HB candidate variables identified in Fig. 3, will be presented in a subsequent paper.

3.1.3. The Giant Branch Intrinsic Color Width

One of the most notable results in the ground-based study of And II by König *et al.* (1993) was their suggestion that And II has a large intrinsic color spread on the giant branch, and thus a significant internal abundance range. In particular, König *et al.* (1993) measured $\sigma_{obs}(g - r) = 0.20$ on the upper giant branch in their c-m diagram. They did not perform a quantitative analysis of their photometric errors but instead estimated them

as $\sigma_{err}(g-r) \approx 0.15$ mag. This in turn yields $\sigma_{int}(g-r) \approx 0.13$ for the intrinsic color dispersion, which they estimate corresponds to $\sigma_{int}([Fe/H]) \approx 0.43$ dex. This value is amongst the largest known for dSph galaxies (e.g. Mateo 1998). Clearly our much smaller photometric errors ($\sigma_{err}(F450W - F555W) \approx 0.02$ at comparable magnitudes) allow us to place much tighter constraints on any intrinsic color range among the giants in this dSph galaxy. That is the subject of this section; we defer to Sect. 3.4 the discussion of the abundance range that results from our determination of the And II giant branch intrinsic color spread.

König *et al.* (1993) considered the giant branch color spread in And II over the interval $22.75 \leq g \leq 23.5$ which corresponds approximately to the interval $22.2 \leq F555W \leq 23.2$. To investigate the intrinsic color spread in this range we first determined a mean giant branch locus by fitting a low order polynomial to the stars in the interval $21.8 \leq F555W \leq 23.8$, excluding a small number of outliers. Then for each of the 85 stars in the interval $22.2 \leq F555W \leq 23.2$, we computed the difference between the $F450W - F555W$ color of the star and that of the mean giant branch at the star's $F555W$ magnitude. The distribution of these differences is shown in Fig. 7. This distribution can be characterized in a number of ways: the standard deviation $\sigma_{obs}(F450W - F555W)$ is 0.12 mag, the inter-quartile range is 0.18 mag, the color range containing the central two-thirds of the sample is 0.27 mag and the full color range of the sample is ∼0.4 mag. All these quantities are considerably larger than the errors in the colors at these magnitudes ($\sigma_{err}(F450W - F555W) \approx 0.02$, cf. Table 1). Indeed the errors are so much smaller than the observed color range at these magnitudes that we can effectively ignore them and regard the observed quantities as intrinsic. Thus we confirm the results of König *et al.* (1993) that the upper giant branch of And II has a significant intrinsic color width. Further, the values of the quantities which characterize the distribution shown in Fig. 7 are all approximately twice as large as the equivalent quantities for the And I intrinsic giant branch color width determined, using similar techniques, in

Paper I (and Appendix A). Thus, while And I and And II have similar total luminosities (Caldwell *et al.* 1992) and similar mean abundances, this does not apply to their intrinsic giant branch color spreads; that of And II is significantly larger.

There are two further comments that are worth making here. First, as noted in Paper I, at these luminosities in Galactic globular clusters, the AGB has either terminated or is no longer distinguishable from the red giant branch. Thus the large intrinsic color width of the And II giant branch is not due to a mixture of AGB and red giant branch stars. Second, there is a hint of bimodality in Fig. 7, which is also evident to some extent in Figs. 3 and 5, though statistically the distribution in Fig. 7 is not significantly different from a gaussian. We shall return to this point in Sect. 3.4.

3.1.4. A Population of "Faint Blue Stars"?

In Paper I we drew attention to the existence in the And I c-m diagram (see also Appendix A) of a population of faint ($V \gtrsim 26.0$) blue ($B - V \lesssim 0.5$) stars. These objects are sufficiently blue that they cannot be easily dismissed as the result of large color errors in subgiant star photometry, and hence they were considered a *bona fide* And I population. There is, however, no compelling evidence for *any* intermediate-age population in And I (Mould & Kristian 1990, Armandroff *et al.* 1993, Armandroff 1994). Thus, in Paper I we interpreted these And I stars as blue stragglers, analogous to those seen in many Galactic globular clusters, rather than as main sequence stars with ages of order 1.5 – 2.5 Gyr.

Because of the shorter exposure times, the limiting magnitudes in Figs. 3 and 5 are not as faint as the equivalent data for And I (cf. Appendix A). Nevertheless, it is apparent from these c-m diagrams that And II also has a recognizable population of faint blue stars. In particular, Table 1 shows that at $F555W \approx 25.8$, the mean repeatability error in

$F450W - F555W$ is approximately 0.11 mag. Thus displacing a subgiant with a true color of $F450W - F555W$ ∼0.6 at this magnitude into the region of the faint blue stars requires a color error of 3 or 4σ. It then seems unlikely that all of the objects with $25.6 \lesssim V \lesssim 26.0$ and $(B - V) \lesssim 0.5$ could be explained in this way.

Visually, when comparing Fig. 3 or Fig. 5 with the equivalent And I c-m diagrams, it appears that And II may contain relatively more of these faint blue stars. We now seek to quantify this impression. Using the data of Fig. 5 there are 39 And II stars with $25.55 \leq V \leq 26.0$ and $(B - V) \leq 0.5$ mag. These stars have an average B of 26.1 mag. Because at these faint magnitudes the degree of completeness is limited by the $F450W$ data (rather than by $F555W$), it is necessary to compare the number of these faint blue stars not with subgiants in the same V mag range, but with a group of subgiants that have a similar mean B magnitude. The interval $25.1 \leq V \leq 25.4$ and $0.70 \leq (B - V) \leq 1.05$ satisfies this requirement: the 87 stars in this interval have $< B > \approx 26.1$ mag. To first order then the selection process should be the same for both groups of stars. If FBS denotes the number of faint blue stars and SG denotes the number of subgiants, then the proportion of faint blue stars of the total $(FBS + SG)$ for And II is 0.31 ± 0.04 assuming Poissonian statistics.

As we shall see in subsequent sections (and in Appendix A), the reddenings and mean metal abundances of And I and And II are similar. The mean magnitude of the horizontal branch, however, is ∼0.3 mag fainter in And I than it is in And II. We can thus calculate a similar proportion for the faint blue stars in And I by adopting the same color limits as for And II but shifting the V magnitude limits 0.3 mag fainter. We find, using the And I data discussed in Appendix A, that $FBS = 49$ and $SG = 186$ stars. The proportion of faint blue stars is then 0.21 ± 0.03, again assuming Poissonian statistics. This lower value for And I confirms the subjective visual impression that And II has relatively more faint blue stars – if the And I proportion applied in And II then we would have expected ∼23 rather

than the observed 39 stars. But is this difference statistically significant? As discussed in Paper I, the appropriate statistic for comparing two proportions is T_2 (see Paper I for the definition), which has a normal distribution with zero mean and unit variance. Using the numbers given above, we find $T_2 = 2.13$ which implies that there is a less than 2% chance that the two proportions are drawn from the same underlying population. This result is not substantially altered by minor changes in the adopted magnitude and color intervals used to define the FBS and SG samples.

As a check on this result we adopt a slightly different approach. On the upper part of the giant branch where completeness issues are not a concern (we used the intervals $23.0 \leq V \leq 23.5$ and $23.5 \leq V \leq 24.0$ for And II, and the equivalent 0.3 V mag fainter intervals for And I; two intervals allowing a consistency check), the number ratio of And II to And I stars in the c-m diagrams is 0.54 ± 0.02. On this basis and using the 49 observed faint blue stars in And I, we expect 26 such stars in And II. In fact we observe 39 such stars, or $\sim$50% more than expected. We conclude then that And II does contain significantly ($\gtrsim$50%) more blue stars, with $M_V \gtrsim +1.2$, than does And I. The nature of these stars will be discussed in Sect. 3.5.3.

3.2. The Distance of And II

In Fig. 5, the mean V magnitude of the 45 blue horizontal branch stars with $24.7 \leq V \leq 25.1$ and $0.05 \leq B - V \leq 0.40$ is 24.93 ± 0.015 (standard error of mean). This value is essentially unaltered for modest changes in the adopted color interval. We thus adopt $V(\mathrm{HB}) = 24.93 \pm 0.03$ for And II, where the uncertainty now includes the adopted error in the aperture corrections ($\pm$0.02) and in the $F555W$ to V transformation zeropoint ($\pm$0.02). In Paper I we found $V(\mathrm{HB}) = 25.25 \pm 0.04$ for And I. Thus it is immediately apparent, given similar reddenings and mean abundances, that And II is $\sim$0.3 mag closer than And I

along the line-of-sight.

To convert the value of V(HB) for And II into a distance, however, we need to adopt both a reddening and a mean abundance, since on our preferred distance scale, the absolute magnitude of the horizontal branch varies with abundance (M_V(HB) = 0.17[Fe/H] + 0.82, cf. Paper I). For the reddening we use the new COBE/DIRBE plus IRAS/ISSA dust maps of Schlegel *et al.* (1998), which allow for extinction fluctuations on smaller angular scales than the earlier work of Burstein & Heiles (1982). At the galactic latitude and longitude of And II, the Schlegel *et al.* (1998) maps yield E($B-V$) = 0.060 mag, somewhat higher than the value E($B-V$) = 0.035 mag given by the Burstein & Heiles (1982) data. We adopt E($B-V$) = 0.06 ± 0.01 and A_V = 0.19 ± 0.03 for And II. The metallicity of And II is the subject of the next section; here we simply adopt the result, <[Fe/H]> ≈ –1.5 ± 0.15 for And II, yielding M_V(HB) = 0.57 ± 0.03 on our adopted distance scale. These data then give (m–M)$_0$ = 24.17 ± 0.06 for And II corresponding to a line-of-sight distance of 680 ± 20 kpc.

To compare this distance with that of M31 requires an M31 distance that is on our adopted distance scale. As discussed in Paper I, there are two such determinations which give somewhat different results. The field halo RR Lyrae and red giant data yield (m–M)$_0$ = 24.40 ± 0.13 (Paper I; see also Lee *et al.* 1993) corresponding to a distance of 760 ± 45 kpc. Alternatively, using our adopted distance scale, the mean horizontal branch magnitudes of the eight M31 globular clusters studied by Fusi Pecci *et al.* (1996) suggest an M31 modulus of (m–M)$_0$ = 24.64 ± 0.05, or a distance of 850 ± 20 kpc. These results then place And II either 80 ± 50 or 170 ± 30 kpc in front of M31 along the line-of-sight. Thus we adopt a relative And II – M31 line-of-sight distance of 125 ± 60 kpc, and note that a more precise value awaits a reduction in the uncertainty in the M31 distance (on our adopted scale). Our result, however, is consistent with the less precise ground-based results

of König *et al.* (1993) who found, via fitting globular cluster giant branches to their c-m diagram, that And II was 120^{+125}_{-100} kpc closer than their adopted M31 distance.

On the sky And II lies closer to M33 than it does to M31 (see, for example, Fig. 2 of Armandroff & Da Costa 1999) suggesting the possibility that And II is associated with that galaxy rather than with M31. However, since M33 lies 0.2 to 0.3 mag beyond M31 (e.g. Lee *et al.* 1993) while And II lies on M31's near side, the association between And II and M31 seems unequivocal.

For our M31 moduli, the projected distance of And II from M31 lies between 135 and 150 kpc. Combining these estimates with the line-of-sight relative distance then indicates that the true distance of And II from the center of M31 lies between ∼160 and ∼230 kpc. The lower value is reminiscent of the Galactocentric distance of the Fornax dSph ($R_G \approx$ 140 kpc) while the upper value is comparable to the Galactocentric distances of the Leo dSphs ($R_G \approx$ 250 and 205 kpc, respectively). The Leo dSphs are the most distant of the Galaxy's system of dSph satellites. And II, however, is probably not the outermost member of the M31 dSph system since the newly discovered M31 dSph companion And VI lies at least ∼270 kpc (the projected distance) from the center of M31 (Armandroff *et al.* 1999).

3.3. The Abundance of And II

The determination of an abundance estimate for And II from these data requires a comparison with the giant branches of standard globular clusters of known abundance. Since there are no giant branch data on the ($F555W$, $F450W - F555W$) system, we must use the And II data transformed to the (V, $B - V$) system. As noted in Sect. 2.1.3, our ground-based photometry suggests that the transformation zeropoint for the B magnitudes, and hence the $(B - V)$ colors, should be altered by 0.055 mag relative to the value given

in H95. It is this zeropoint corrected photometry (cf. Fig. 5) that we adopt here. The standard globular cluster giant branches are those for the Galactic globular clusters M68 ([Fe/H]=–2.09), M55 ([Fe/H]=–1.82), NGC 6752 ([Fe/H]=–1.54), NGC 362 ([Fe/H]=–1.28) and 47 Tuc ([Fe/H]=–0.71) as described in Paper I. In particular, the globular cluster abundances are taken from Armandroff (1989) and are on the Zinn & West (1984) system. For And II we adopt the Schlegel *et al.* (1998) reddening $E(B-V) = 0.06$ and use $A_V = 0.19$ mag.

Since we employ a distance scale that depends on abundance, the determination of the mean abundance, via the comparison with standard globular cluster giant branches, and the determination of the distance modulus, are necessarily interconnected. In brief, we first assumed an estimate for the mean abundance, which then allows the calculation of an And II apparent distance modulus. This permits the globular cluster giant branches to be overlaid on the And II photometry and a new estimate for the mean abundance can be determined (see below). The new mean abundance then yields a new modulus and the cycle is repeated; convergence is rapidly achieved. We show the result of this process in Fig. 8, in which the (V, $B-V$) photometry of Fig. 5 is presented with the standard globular cluster giant branches superposed using the final adopted And II modulus.

To determine the mean abundance we computed mean $(B-V)$ colors for the stars, excluding obvious outliers, that lie in a series of 0.2 V mag wide bins. There were six bins on the upper giant branch between $V = 22.15$ and $V = 23.35$ and two bins on the lower giant branch between $V = 25.15$ and $V = 25.55$. In this latter case the magnitudes are fainter than that of the horizontal branch. As discussed in Paper I, the lower giant branch offers the advantage of a larger sample and freedom from contamination by stars evolving from the horizontal branch. However, at these fainter magnitudes the photometric errors are larger and the possibility of contamination from non-member objects is greater.

The reduced sensitivity to abundance also means that small color uncertainties can result in large abundance errors. On the other hand, at higher luminosities, while sample sizes are smaller, the photometric errors are also smaller (cf. Table 1). Further, the range in color corresponding to a given abundance interval is larger and thus any small systematic uncertainties in the colors become less important. The largest potential disadvantage of using the upper giant branch, however, is contamination from asymptotic giant branch (AGB) stars, which are generally hotter than red giant branch (RGB) stars of similar luminosity and abundance. Fortunately, as noted in Paper I, in the c-m diagrams of the standard globular clusters (see Paper I for the individual references) AGB stars cease to be readily distinguishable from RGB stars brighter than $M_V \approx -1.5$ or $V \approx 22.9$ in And II.

The abundances were determined from the mean colors for each bin by applying the abundance calibration for that bin. These calibrations were determined by least squares fits (linear for all but the three most luminous bins where quadratic relations were used) to the colors of the giant branches of the standard clusters at the V magnitudes of the bin centers, and the known abundances of the clusters. For the two lower luminosity bins, which contain samples of 60 and 80 stars, respectively, the mean abundance determined is $<$[Fe/H]$> = -1.32 \pm 0.06$, where the error given reflects solely the uncertainty in the abundance resulting from the statistical uncertainties in the mean colors. For the six bins on the upper giant branch, where the sample sizes range from 12 to 26 stars per bin, the mean abundance determined is $<$[Fe/H]$> = -1.49 \pm 0.04$ dex. Again the error here is just that resulting from the statistical uncertainty in the mean colors. For these upper giant branch bins there is no sign of any trend between the individual $<$[Fe/H]$>$ values and V indicating, as expected, that the inclusion of AGB stars has not biased these abundance estimates.

The abundance error due to the statistical uncertainty in the mean colors is, of course,

not the only uncertainty in the abundance estimates. A full accounting should include the effects of uncertainty in the $(B-V)$ zeropoint, which we take as ± 0.03 mag, uncertainty in the distance modulus, which we take as ± 0.06 mag (i.e. we exclude any systematic uncertainty in our adopted distance scale), together with uncertainty in the abundance calibration process itself. This latter uncertainty we take as the rms deviation about the least squares fits, which are of order 0.05 dex for both the upper and lower giant branch. For the upper giant branch mean abundance determination, no single uncertainty significantly exceeds any other and the quadratic sum of the contributions is 0.11 dex. That is, the upper giant branch estimate of the mean abundance of And II is <[Fe/H]> = –1.49 ± 0.11 dex. For the lower giant branch the $(B-V)$ zeropoint uncertainty dominates and the total error is 0.20 dex; i.e. the lower giant branch estimate of the mean abundance is <[Fe/H]> = –1.32 ± 0.20 dex.

The difference, 0.17 dex, in the sense of a lower abundance mean found from the upper giant branch, is reminiscent of a similar difference found for And I in Paper I (see also Appendix A). We prefer to adopt the mean abundance determined from the upper giant branch for the principal reason that our calibration of the $(B-V)$ zeropoint, on which the abundance determination ultimately rests, is predominantly based on upper giant branch stars (cf. Fig. 4). Further, at fainter magnitudes the fiducial giant branches for the standard globular clusters are not as precisely defined as they are at luminosities above the horizontal branch. Thus, when combined with the large change in abundance produced by small color differences at these magnitudes ($\Delta([\mathrm{Fe/H}])/\Delta(B-V) \approx 5.3$), this effect might be sufficient to generate the systematic offset.

We therefore adopt <[Fe/H]> = –1.49 ± 0.11 dex as our best estimate of the mean abundance of And II. This value is in good agreement with the less precise value of <[Fe/H]> = –1.59 $^{+0.44}_{-0.12}$ determined by König *et al.* (1993) from their ground-based (g,

$g - r$) photometry. It is also in very good agreement with the recent spectroscopic And II mean abundance given by Côté *et al.* (1999b). These authors used line indices measured from low resolution Keck spectra of ∼40 And II red giants to determine <[Fe/H]> = –1.47 ± 0.19 dex. Our value for the And II mean abundance is also closely similar to the new mean abundance for And I, <[Fe/H]> = –1.46 ± 0.12 dex, derived in Appendix A. As noted above, these M31 dSph companions have closely similar luminosities (Caldwell *et al.* 1992).

One final point deserves mention. To investigate whether or not there might be a radial abundance gradient in And II, we split the data as described in Sect. 3.1.1 and computed mean abundances for the radially selected samples from the giant branch colors. For both the samples inside and outside the core radius, and inside and outside the elliptical boundary that divides our total sample approximately in half, we see no evidence to suggest the presence of any abundance gradient. The 3-σ upper limit on the size of any such gradient is ∼0.3 dex within ∼1.3 core radii; larger samples of red giants in the outer regions of this dSph are required to generate a stricter limit. This result is consistent with those for other dSphs (e.g. Paper I) – in no dSph system is the existence of a radial abundance gradient firmly established.

3.4. The Abundance Spread in And II

In section 3.1.3 we demonstrated that the And II giant branch has a significant intrinsic color width. The abundance calibration established in the previous section can now be used to convert this intrinsic color width into an abundance distribution. Specifically, we make use of the 108 stars in the 6 upper giant branch V mag bins employed to determine the And II mean abundance. By applying the appropriate abundance calibration to each individual star in each bin, we are able to generate 108 individual [Fe/H] values. However,

before collecting these values into an abundance distribution, it is first necessary to estimate the uncertainty in these individual values.

In this V magnitude range, Table 1 shows that the mean error in the $F450W - F555W$ colors is ≤ 0.02 mag. Then noting that $\Delta(B-V)/\Delta(F450W - F555W) \approx 1.25$ and that $\Delta[Fe/H]/\Delta(B-V) \approx 2.5$ for these giant branch stars, the uncertainty in the individual abundance determinations is approximately σ_{err}([Fe/H]) $\lesssim 0.08$ dex. We have therefore adopted a bin size of 0.15 dex in generating histograms for the And II abundance distribution (as inferred from these giant branch stars). The distribution is shown as the solid lines in the panels of Fig. 9, where the upper and lower panels of the figure show the result of offsetting the origin of the abundance bins by one half of a bin width.

The observed abundance distribution shown in Fig. 9 can be characterized in a number of ways. For example, the standard deviation σ_{obs}([Fe/H]) is 0.36 dex, the inter-quartile range is 0.66 dex, the abundance range shown by the central two-thirds of the sample is 0.80 dex and the full abundance range is approximately 1.4 dex. The contribution from the photometric errors, σ_{err}([Fe/H]) ≈ 0.08 dex, is negligible by comparison and thus we can take all these quantities as intrinsic. In particular, we have σ_{int}([Fe/H]) = 0.36 dex. This value is somewhat smaller than the value, σ_{int}([Fe/H]) ~ 0.43 dex, derived by König *et al.* (1993) from their ground-based photometry of the And II giant branch, but given the much larger photometric errors in that study, the agreement is quite satisfactory. Our result is also again in excellent agreement with that of Côté *et al.* (1999b), who derive σ_{int}([Fe/H]) $= 0.35 \pm 0.10$ dex from the dispersion of Mg b line strength indices in their low resolution spectra of approximately 40 And II red giants. These authors also estimate σ_{int}([Fe/H]) $\approx 0.46 \pm 0.17$ from the dispersion in their $(V-I)$ giant branch colors.

How do these And II results compare with the intrinsic abundance dispersions in the other M31 dSph companions? For the recently discovered systems And V, And VI (Peg

dSph) and And VII (Cas dSph), the limited information available lacks sufficient precision for useful comparisons. Armandroff *et al.* (1999) indicate that σ_{int}([Fe/H]) $\sim$ 0.3 dex for And VI based on their ground-based V, I photometry, although they did not carry out a full analysis of their photometric errors. On the other hand, Grebel & Guhathakurta (1999) indicate only that "the observed width of the RGB" in the Peg (And VI) and Cas (And VII) dSphs "corresponds to a metallicity spread of roughly 1 dex". This leaves And I (Paper I, see also Appendix A) and And III (Armandroff *et al.* 1993) as the only suitable comparison objects. For And I the analysis in Appendix A was carried out using similar WFPC2 data and the same technique. Although this dSph has a similar total luminosity and central surface brightness to And II, and a similar mean metallicity, the abundance distribution in And II is significantly broader than it is in And I. This is illustrated in Fig. 9 where the abundance distributions of the two dSphs are directly compared. Quantitatively, σ_{int}([Fe/H]) $\approx$ 0.21 for And I while it is 0.36 dex for And II. Similarly, the inter-quartile range is 0.36 dex versus 0.66 for And II, and the central two-thirds of the sample range is 0.49 dex in And I compared to 0.80 dex for And II. *Thus, despite resulting in similar mean abundances, the chemical enrichment processes in these two dSphs must have been significantly different.* The less luminous M31 dSph And III also shows an intrinsic abundance dispersion that is considerably less than that for And II; Armandroff *et al.* (1993) give $0.16 \leq \sigma_{int}([\mathrm{Fe/H}]) \leq 0.24$ from their ground-based V, I photometry. As for Galactic dSphs, based on the compilation of Mateo (1998) and the references therein, only the Fornax and Sagittarius dSphs have intrinsic abundance dispersions that convincingly exceed that of And II. Both these dSphs, however, are at least two magnitudes more luminous than And II.

The And II abundance distribution shown in Fig. 9 is sufficiently broad compared to the abundance uncertainties that it is worth investigating the implications of the observations through the use of simple chemical enrichment models (cf. Zinn 1978, Norris *et*

al. 1996). In particular, this process may shed some light on the hint of bimodality seen in Fig. 9 (cf. Fig. 7). Of course in reality the chemical evolution of a dSph galaxy is a complex process involving the effect of star formation driven processes, particularly supernovae, on the distribution and chemical composition of the gas that resides within the dark matter potential of the dSph. Detailed models of these processes (e.g. Larson 1974; Dekel & Silk 1986; Vader 1986, 1987; Mac Low & Ferrara 1999) are, however, necessarily heuristic in nature and therefore do not readily supply an interpretative guide for individual objects in the way simple models do.

The simplest models are those in which the assumption of instantaneous recycling is made (e.g. Tinsley 1980). The metallicity distribution function $f(z)$ can be then written as:

$$f(z) \; = \; (1/y)\, exp\,[-(z - z_0)/y] \qquad z \geq z_0 \tag{1}$$

Here z_0 is the initial abundance and y is the "yield". The relationship between the yield and the mean abundance then depends on how the gas is lost from the system. If the rate of gas loss is assumed to be directly proportional to the star formation rate ("steady gas loss", e.g. Hartwick 1976), then the yield and the mean abundance, $<z>$, have the simple relation $y = <z> - z_0$. The abundance distribution for such simple models then has two parameters, $<z>$ and z_0. An alternative (cf. Zinn 1978) is "sudden gas loss" where the evolution is terminated when the abundance reaches $z = z_{max}$. In this case the mean abundance $<z>$ is again related to y, z_0 and z_{max} and we can employ equation (1) for $z_0 \leq z \leq z_{max}$ with $f(z) = 0$ otherwise. The abundance distribution for these models then has three parameters; z_0, z_{max} and y (or $<z>$).

The left panels of Fig. 10 show examples of these types of models compared with the And II observations. In each case the distribution function $f(z)$ was integrated over the same set of abundance bins as the observations and then normalized to the total number of stars. While we have not thought it worthwhile to carry out any parameter

optimization via, for example, a maximum likelihood analysis, the models shown are likely to be representative of the "best fit" that can be achieved with models of this type. The steady gas loss model shown is for $\log(< z >/z_{sun}) = -1.35$ and $\log(z_0/z_{sun}) = -2.05$ where we have adopted $z_{sun} = 0.02$. For the sudden gas loss model $\log(< z >/z_{sun}) = -1.40$, $\log(z_0/z_{sun}) = -2.05$ and $\log(z_{max}/z_{sun}) = -0.75$.

While these simple models do show reasonable agreement with the observations, the actual fits are not very satisfactory. The models tend to have rather too many stars at intermediate abundances and rather too few at the extremes compared to the observed distribution. We have therefore investigated a simple extension of these models (cf. Norris *et al.* 1996) in which we have allowed for the possibility of *two* components, both following the steady gas loss formalism. Such a combination has five parameters: z_0 and $< z >$ for each component and the relative strength of the two components. Again we have not attempted to find the optimum fit but show in the right panels of Fig. 10 an illustrative example which certainly provides better agreement with the observations than the single component models. This model has $\log(< z >/z_{sun}) = -1.6$ and $\log(z_0/z_{sun}) = -2.05$ for the "metal-poor" component and $\log(< z >/z_{sun}) = -0.95$ and $\log(z_0/z_{sun}) = -1.20$ for the "metal-rich" component with metal-poor component stars outnumbering metal-rich ones by 2.3 to 1. We note also that a two component sudden gas loss model gives an almost identical representation of the data using similar values for the mean abundances of the two components and their number ratio.

We therefore conclude that the broad abundance distribution in And II, at least in the context of simple enrichment models, is best understood in terms of *two* components each with an intrinsic abundance range. The mean abundances of these components differ by $\sim$0.6 dex and their number ratio is approximately 2.3 to 1 (metal-poor to metal-rich). This situation is reminiscent of that in the Galactic globular cluster ω Cen, where Norris *et al.*

(1996) find that the [Ca/H] distribution among the cluster red giants suggests the presence of two components whose mean [Ca/H] values differ by ∼0.5 dex. It is also interesting to note that recently Majewski *et al.* (1999) have suggested that the metallicity distribution function in the Galactic dSph Sculptor is bimodal, with the two components differing in mean abundance by ∼0.8 dex. Taken *in toto* then, these and other available results for dSph abundance distributions (e.g. Smecker-Hane *et al.* 1999) serve to remind us yet again of the complex and diverse evolutionary histories these purportedly simple systems have undergone.

3.5. The Age(s?) of And II

The existence of blue horizontal branch and RR Lyrae variable stars in And II immediately testifies to the existence of an old (age > 10 Gyr) population in this dSph galaxy. This is not a surprising result since, although the relative proportion of old stars varies significantly from dSph to dSph, all Local Group dSph galaxies studied in sufficient detail contain an old population[5].

The blue horizontal branch (HB) stars make up ∼20% of the total And II HB population (cf. Sect. 3.1.1), and we can take this percentage as an approximate lower limit on the fractional size of the old population in And II. Nevertheless, the bulk of the HB stars in And II are red and thus potentially of younger age. However, we have already seen (cf.

[5]The one possible exception to this statement is the Galactic companion dSph Leo I in which 70 – 80% of the star formation activity occurred between ∼7 and ∼1 Gyr ago (e.g. Gallart *et al.* 1999a). The detailed modelling of Gallart *et al.* (1999b), however, does not unambiguously rule out the existence of a ∼12 – 15 Gyr old population in Leo I, though any such population must be small.

Sect. 3.4) that And II has a substantial internal abundance spread. Consequently, at least in principle, significant numbers of red HB stars could be contributed by a relatively metal-rich old population, lessening the need for any younger stars. Thus we need to investigate whether the And II HB morphology can be explained by an appropriate combination of standard Galactic globular cluster HB morphologies, given the consequent implication that most And II stars would have ages similar to those of the Galactic globular clusters.

3.5.1. Modelling the Horizontal Branch Morphology

To approach this question we have chosen to use published data for Galactic globular clusters with known (old) ages rather than employ sets of theoretical isochrones. This is principally because theoretical isochrones (at fixed age and abundance) do not reproduce the spread in color (temperature) on the horizontal branch in real globular clusters without invoking variable amounts of mass loss from the red giant branch progenitors. On the other hand, to be of use in this simulation, where we will combine appropriately scaled (in star number) c-m diagrams of globular clusters of differing metal abundance, the cluster data needs to be essentially complete to magnitudes fainter than that of the horizontal branch. We have used the photometry of M55 ([Fe/H] = –1.82) from Lee (1977b), of NGC 1851 ([Fe/H] = –1.29) from Walker (1992; specifically the data for his Fig. 4) and of 47 Tuc ([Fe/H] = –0.71) from Lee (1977a; specifically the data for his Ring 6). For all three of these cluster data sets the ratio of the number of bright red giants to the number of horizontal branch stars is virtually the same, indicating similar completeness levels. Likely field objects that lie far from the fiducial sequences have been removed as have known RR Lyrae stars from the M55 and NGC 1851 photometry.

M55 is a "standard" metal-poor globular cluster with a strong blue HB morphology, while 47 Tuc is the archetypal relatively metal-rich globular cluster with a pure red HB

morphology. NGC 1851 has a somewhat anomalous HB morphology in that the distribution of HB stars is approximately bimodal: there are significant numbers of red and blue HB stars but a relative deficiency of RR Lyrae variables (see Fig. 7 of Walker 1992). However, the ages of all three clusters, based on main sequence turnoff photometry, appear to be typical in the sense that they are not notably younger (or older) than other clusters with similar abundance. For example, none of these three clusters are distinguished in Fig. 1 of Chaboyer *et al.* (1996).

To combine these c-m diagrams we first shifted the observed cluster data to our adopted And II reddening and distance modulus. We then split the And II abundance distribution of Fig. 9 into three groups: –2.2 ≤ [Fe/H] ≤ –1.6 to be represented by M55, –1.6 ≤ [Fe/H] ≤ –1.0 to be represented by NGC 1851, and –1.0 ≤ [Fe/H] ≤ –0.5 to be represented by 47 Tuc. These groups contribute 44, 45 and 11 percent of the total. The numbers of stars in the M55 and 47 Tuc samples were then scaled so that the numbers of bright red giants (we adopted $V \leq 23.5$) for these clusters were in the correct proportion to the bright red giant numbers in the NGC 1851 sample. The resulting c-m diagram is shown in the upper panel of Fig. 11. Converting the $F450W - F555W$ color limits for the HB morphology index i (cf. Sect. 3.1.1) to $B - V$, we find $i = 0.46 \pm 0.03$ for this composite globular cluster sample. For And II, using the sample excluding the candidate variable stars (i.e. Fig. 5), the value of the index is $i = 0.17 \pm 0.02$, a significantly lower value ($T_2 = 8.3$). We therefore conclude that the HB morphology of And II cannot be modelled by the appropriate combination of HB morphologies of "standard" globular clusters.

To reproduce the And II HB morphology index, it is necessary to reduce the numbers of blue HB stars in the upper panel of Fig. 11 and to increase the numbers of red HB stars. To do this we have removed all of the NGC 1851 blue HB stars and ∼45% of the M55 blue HB stars and replaced them with red HB stars. These red HB stars were taken from the

NGC 362[6] ([Fe/H] = –1.28) c-m diagram of Harris (1982, all listed red HB stars) and, since there were insufficient stars in the NGC 362 c-m diagram to make up the required numbers, from the 47 Tuc data for the remaining $\lesssim$20 percent. No changes were made to any non-HB stars. The c-m diagram with this modified HB morphology is shown in the lower part of Fig. 11. It has a HB morphology index i value identical to that for And II.

Thus to summarize this analysis, we find that in order to reproduce the HB morphology of And II, we have to convert $\sim$65% of the total HB population generated from an appropriate combination of "standard" globular clusters from blue into red HB stars. Consequently, like many of the Galactic dSphs and like And I (Paper I) we can classify And II as a "second parameter" object.

The interpretation of this second parameter remains controversial, at least for Galactic globular clusters. On the one hand, Stetson *et al.* (1999) have shown that the outer Galactic halo second parameter clusters Pal 3, Pal 4 and Eridanus are indeed younger than their standard globular cluster counterparts M3 and M5. Yet on the other hand, recent results for globular clusters in the Fornax dSph (Buonanno *et al.* 1998) and in the LMC (see the discussion in Da Costa 1999), for example, appear to indicate that age is not the only (second) parameter in determining HB morphologies. However, for dSphs the interpretation of second parameter HB morphologies as the result of younger-aged populations is less controversial. There are at least two reasons for this. First, dSphs are very low density systems when compared to globular clusters. Hence any dynamical

[6]NGC 362 is well known to be a "second parameter" cluster in that its HB morphology is redder than expected for its abundance. Despite the continuing controversy surrounding the interpretation of the second parameter for Galactic globular clusters, it does seem that in the case of NGC 362 at least, the red HB morphology is caused by a younger age (e.g. Green & Norris 1990).

effects that could generate HB morphology changes will be insignificant. Second, among the Galactic dSphs, the second parameter nature of the horizontal branch morphologies has, in most instances (e.g. Carina, Fornax, Leo I and Leo II), been shown by main sequence turnoff photometry to result from significant stellar populations that are younger (and in some systems substantially younger) than Galactic halo globular clusters.

There are, however, two apparent exceptions to this "age is the second parameter for dSphs" interpretation. The first of these is the low luminosity, metal-poor Galactic dSph Draco. Grillmair *et al.* (1998) find from main sequence turnoff photometry obtained with WFPC2 that the Draco stellar population in the small field imaged is 1.6 ± 2.5 Gyr older than the Galactic halo globular clusters M68 and M92. Modulo possible calibration uncertainties (cf. Sect. 3.2 of Grillmair *et al.* 1998), this result contradicts, at the $\sim 1.4\sigma$ level, the expectation based on the respective HB morphologies and a strict "age is the second parameter" interpretation, that Draco should be ∼2 Gyr younger than these globular clusters. The second exception is the Galactic dSph Sculptor where the new ground-based photometry of Hurley-Keller *et al.* (1999) demonstrates vividly the HB morphology gradient in this dSph, previously discussed in Paper I, in which the red HB stars are more centrally concentrated than the blue HB stars. However, at a 1–2 Gyr level of precision, Hurley-Keller *et al.* (1999) do not see the corresponding ∼2 Gyr change in the mean age of the population that is required if age was solely responsible for the change in HB morphology.

Despite these two possible exceptions, by analogy with the majority of Galactic dSphs, we interpret our results for the HB morphology in And II as indicating that at least ∼50% of the total population in this dSph has an age or ages less than that of the Galactic globular clusters. Is there any independent evidence to support this conclusion? In the case of And II there is, since, as mentioned in the Introduction, there are claims of stars in And II with luminosities considerably above that of the first giant branch tip. Such

upper-AGB stars are likely to be of intermediate (1 – 10 Gyr) age. We now look at those claims in more detail.

3.5.2. The Case for an Intermediate-Age Population

Aaronson *et al.* (1985) spectroscopically identified three candidate upper-AGB stars in And II. These are the "marginal carbon star" A10, the M0 star A209 and the carbon star A211. Unfortunately A209 and A211 fell in the vignetted region between the WF3 and WF4 frames and so we are unable to include them in our c-m diagrams. Similarly, A10 is outside the WFPC2 field. Nevertheless, we can calculate the bolometric magnitudes for these stars using: (a) the original Aaronson *et al.* (1985) near-IR photometry corrected to our And II modulus, and (b) the (I, $V-I$) photometry of Côté *et al.* (1999b) using bolometric corrections from Da Costa & Armandroff (1990) and our And II distance modulus. We can also utilize unpublished And II (I, $V-I$) CCD photometry obtained with the 4 m telescope at Kitt Peak (see Armandroff 1994). Considering first the most luminous star A209, which is of type M rather than type C, the bolometric magnitude values are –4.3, –4.8 and –4.4, respectively, from the above sources. In particular, the Côté *et al.* (1999b) and the KPNO photometry differ by $\Delta(V) = -0.23$ and $\Delta(I) = -0.37$ mag (sense is Côté *et al.* minus KPNO), so it is quite probable that star A209 is a variable, probably of the long period type (LPV). Such stars are not necessarily of intermediate-age. As shown by Frogel & Elias (1988; see also Guarnieri *et al.* 1997 and the discussion in Sect. 7.2 of Caldwell *et al.* 1998), in Galactic globular clusters with abundances [Fe/H] $\gtrsim$ –1.0 the Long Period Variables can have luminosities as bright as $M_{bol} \approx -4.6$ (e.g. V7 in NGC 6712 at [Fe/H] = –1.01, or V2 in 47 Tuc at [Fe/H] = –0.71) yet there is no suggestion that such clusters are of intermediate-age. Since we have established that there is a population with [Fe/H] $\gtrsim$ –1.0 in And II (cf. Fig. 9), there is no requirement to regard star A209 as an intermediate-age

object.

For the stars with carbon star spectral signatures, the M_{bol} estimates range from –3.9 to –4.3 for A10 and suggest $M_{bol} \approx$ –4.0 for A211. Again it is likely that both these stars are variable: in the same sense as above $\Delta(V) =$ –0.07 and $\Delta(I) =$ –0.23 for A10 and $\Delta(V) = +0.49$ and $\Delta(I) = +0.12$ mag for A211. Nevertheless, the bolometric magnitudes do place these stars above the RGB tip ($M_{bol} \approx$ –3.6) and when coupled with the observed indications of third dredge-up material in their surface layers, argue convincingly that they do belong to an intermediate-age population in And II. In particular, all star clusters containing stars showing evidence of the third dredge-up process (i.e. carbon and S-type upper AGB stars) have main sequence turnoff ages less than ∼10 Gyr. Similarly, those Galactic dSphs with upper-AGB carbon stars also have established main sequence populations of intermediate-age.

The luminosities of the And II carbon stars are, however, somewhat lower than their counterparts in Galactic dSphs. Azzopardi (1994) lists $M_{bol} \approx$ –4.4, –4.5, –4.6 and –5.6 for the brightest carbon stars in the Leo II, Leo I, Carina and Fornax dSph galaxies. Of these systems Leo II contains the oldest intermediate-age population: Mighell & Rich (1996) conclude from WFPC2 photometry of the main sequence turnoff that it contains only stars older than ∼7 Gyr with a "typical" member having an age of ∼9 Gyr. While two stars is far from sufficient to establish the AGB termination luminosity in And II (and thus the minimum age of the intermediate-age population) it seems likely that this age is nearer to ∼6–9 Gyr than it is to ∼1–3 Gyr.

Côté *et al.* (1999b) list two additional candidate And II intermediate-age stars from their spectroscopic and photometric study: stars 14 and 30 in their list, both of which are radial velocity confirmed members. For star 14 the Côté *et al.* (1999b) (I, $V - I$) photometry yields $M_{bol} \approx$ –4.5 on our adopted modulus but spectroscopically it is of type

M (the spectrum reproduced in Fig. 2 of Côté *et al.* 1999b suggests a spectral type of M3 or M4 III). Thus star 14 is similar to A209 and is not required to be of intermediate-age. The second object (star 30) has $M_{bol} \approx -4.1$ and possesses a relatively featureless spectrum that rules out a C or M classification (not surprising given the star's relatively blue $V-I$ color). Unlike star 14 which lies some distance from the dSph's center, star 30 is within the field imaged with WFPC2. We find it to be 0.44 mag fainter in V than do Côté *et al.* (1999b). Furthermore, this star is one of the two at the RGB tip in Fig. 3 that are classified as possible variables (the two $F555W$ magnitudes differ by –0.09 mag). Star 30 is then clearly a variable which may have been near maximum light at the epoch of the Côté *et al.* (1999b) photometry. Again it is not necessary to classify it as being of intermediate-age, though it could well be.

Besides star 30, there are five other stars in common between our data set and the spectroscopically observed sample of Côté *et al.* (1999b): stars 3, 4, 5, 6 and 32. The V photometry of Côté *et al.* (1999b) agrees reasonably well with our WFPC2 data for stars 4 and 6 where the $\Delta(V)$ values, in the sense (Côté *et al.* – WFPC2) are –0.08 and –0.04 mag, respectively. For star 32 $\Delta(V) =$ –0.21, but inspection of the WFPC2 frames suggests that the ground-based photometry could have been influenced by a nearby companion. Star 5 is the second of the RGB tip candidate variables flagged in Fig. 3 where the two $F555W$ magnitudes differ by +0.08 mag. However, the Côté *et al.* (1999b) V magnitude and the mean of the WFPC2 values differ only by –0.07 mag (same sense as before) so that the case for this star being a variable is not strong. The final star in common is star 3, which Côté *et al.* (1999b) have shown is a carbon star with strong C_2 bands in its spectrum. Our V magnitude is 0.20 mag fainter than that given by Côté *et al.* (1999b) and thus this star is also likely to be a variable. However, despite its carbon star type spectrum, its luminosity ($M_{bol} \approx -3.45$ from the Côté *et al.* photometry) lies below that of the RGB tip and thus once again it is not necessary to classify this star as an intermediate-age object (Côté *et*

al. 1999b). Near-infrared photometry would be worthwhile to confirm the relatively faint bolometric magnitude.

To summarize then, the case for an intermediate-age population in And II rests on the second parameter nature of at least half the horizontal branch population and on the above-the-RGB-tip luminosity of the Aaronson *et al.* (1985) carbon and marginal-carbon stars A211 and A10. An extensive survey for additional upper-AGB carbon stars in And II is needed to progress the question further.

3.5.3. The Nature of the Faint Blue Stars

We now consider the faint blue stars discussed in Sect. 3.1.4. In Fig. 12 isochrones from Bertelli *et al.* (1994) are shown superposed on the And II observations using our adopted reddening and distance modulus. The isochrones are for abundances $\log(z/z_{sun}) = -1.3$ and –0.7 dex, and for ages between 1.25 and 2.5 Gyr. This figure shows that the location of these faint blue stars in the And II c-m diagram is consistent with the interpretation that they represent the tip of a main sequence population whose youngest age is of order 1.5 Gyr. Although we have not carried out any quantitative completeness analysis, it is likely that the photometry presented in Fig. 12 is becoming seriously incomplete by $V \approx 26.0$ (and $B \approx 26.7$). Thus it is quite possible that there are substantially more of these stars at $V \gtrsim 26.0$ mag. Such stars would be either unevolved main sequence stars of age ∼1.5 Gyr or a main sequence turnoff population that is somewhat older.

Is this "younger main sequence" interpretation of these faint blue stars reasonable? Perhaps, though the apparent lack of upper-AGB carbon stars with $M_{bol} \approx -4.5$ or brighter suggests that any ∼1.5 – 2.5 Gyr population cannot be a large contributor to And II's overall make-up. Nevertheless, it is intriguing that we see relatively more of these faint

blue stars in And II than in And I (cf. Sect. 3.1.4) and it is And II where there are definite indications of an intermediate-age population that is lacking in And I. We note for completeness that for a population older than ∼6 Gyr, which might provide the progenitors for the observed And II upper-AGB carbon stars, the turnoff magnitude is fainter than $V \approx 27.7$, well below the detection threshold of the current data.

An alternative interpretation of these faint blue stars (cf. Paper I) is that they represent a blue straggler sequence arising from a postulated age $\gtrsim 6$ Gyr population. Blue stragglers are known to occur in low central concentration globular clusters so there seems no *a priori* reason why they should not also be found in dSph galaxies. Indeed, if blue stragglers are related to binaries, as seems likely, then the high binary star frequency inferred for the Draco and Ursa Minor Galactic dSphs by Olszewski *et al.* (1996), which is considerably higher than that for both Population I and Population II samples, would almost require the existence of blue straggler stars in dSph galaxies. Further, Hurley-Keller *et al.* (1999) have offered a high binary fraction as the most reasonable explanation of an unusual "spur" of stars observed in their c-m diagram for the Sculptor dSph. At $V \approx 25.8$ or $M_V \approx +1.4$, the brightest of the faint blue stars in And II are somewhat brighter than the brightest of the Galactic globular cluster blue straggler stars, but as noted in Paper I this is probably not a serious concern. If there is a prominent And II population with an age less than that of the Galactic globular clusters, then the turnoff masses are correspondingly higher and this presumably permits somewhat more massive, and thus more luminous, blue straggler stars.

Unfortunately, a decision between these two interpretations of the And II faint blue star population cannot be made without significantly deeper photometry, whose acquisition represents a challenging task indeed.

4. Discussion

With HST/WFPC2 data now available for two of M31's six known dSph companions, and new ground-based data appearing for the others (e.g. Caldwell 1999 and references therein) we can begin to compare the properties of the M31 dSph system with those of the Galaxy's dSph satellite system in some detail, seeking to identify any differences that could be ascribed to the different environments of the dSph systems (cf. Armandroff 1994, Armandroff & Da Costa 1999). In particular, M31 and the Galaxy are generally regarded as being quite similar, with the major difference being M31's higher luminosity. However, Freeman (1999a) argues that the stellar halos and bulges of these two galaxies are, in fact, fundamentally different. M31 has a relatively metal-rich bulge with an $r^{1/4}$ law light profile that dominates any metal-poor halo population at all radii (as in giant ellipticals). This bulge probably formed rapidly via violent collapse or early merger (Freeman 1999a). The Galaxy, on the other hand, has a relatively metal-poor halo with a light profile $\rho_{\rm L} \propto r^{-3.5}$ in which accretion of small satellite systems has probably played a significant role, particularly in the early stages of halo formation. Further, the Galaxy's bulge is small, boxy and probably bar-like; it may have formed from the disk via dynamical instabilities (Freeman 1999a). Thus, in the present context, M31 and the Galaxy can be said to have provided different "parental" environments for their dSph systems.

We note first then that, as shown in Caldwell (1999) for example, the Galactic and M31 dSphs follow essentially identical relations between central surface brightness, absolute magnitude and mean abundance. This result is reinforced if (minor) adjustments are made to the location of the And I and And II points in the diagrams of Caldwell (1999) to account for the mean metal abundance determinations presented here (cf. Sect. 3.3), and for the smaller distance modulus found for And II in Sect. 3.2.

There are only three significant outliers in these relations, as depicted in Figs. 3 and 4 of

Caldwell (1999). The most blatant of these is the Galactic dSph Leo I which has a notably higher central surface brightness for its mean metal abundance or absolute magnitude when compared to the relation followed by the other dSph galaxies. This discrepancy may be related to Leo I's dominant relatively young population (e.g. Gallart *et al.* 1999a, b) although, since Leo I is less of an outlier in the M_V, <[Fe/H]> plane, simple fading does not remove the discrepancy. The second outlier is the Fornax dSph, whose published mean metallicity of approximately –1.4 dex (Buonanno *et al.* 1985, Beauchamp *et al.* 1995) is too low by ∼0.2 dex for this dSph's absolute magnitude. The significance of this deviation from the mean relation is not high, but here again the explanation may lie with the stellar population. Fornax has a substantial intermediate-age population (e.g. Stetson *et al.* 1998 and references therein) and this will generate a bluer mean giant branch color (for a given abundance), which could then be incorrectly interpreted as a lower mean abundance when compared with standard globular cluster giant branches. A spectroscopic mean abundance determination for Fornax would aid in resolving (or confirming) this discrepancy. The third outlying object is And V. For this dSph the mean abundance (<[Fe/H]> ≈ –1.5, no error listed) derived by Armandroff *et al.* (1998) from their c-m diagram study is too high by ∼0.5 dex for the central surface brightness and absolute magnitude determined by Caldwell (1999). And V is a Cycle 8 target for observing with HST/WFPC2 and it will be interesting to see if the new data confirm the relatively high abundance found by Armandroff *et al.* (1998). If it does, And V will become the first dSph to clearly deviate significantly from the M_V, <[Fe/H]> relation followed by the other galaxies. Nevertheless, despite these possible outliers, the similarity of the relations between central surface brightness, absolute magnitude and mean abundance for the M31 and Galactic dSphs indicates that these relations are not strongly influenced by the properties of the parent galaxy.

As regards horizontal branch morphologies, seven of eight Galactic dSphs can be classified as "second parameter" objects in that they possess redder HB morphologies

than most Galactic globular clusters of abundance similar to the dSph means. The sole exception is the Ursa Minor dSph which has a blue HB morphology consistent with its low mean abundance (the HB morphology and mean abundance of the Sagittarius dSph are not yet well established, so it is not included here). With the And II results presented in this paper, we now have HB morphologies for two of the six M31 dSph companions. Like the vast majority of the Galactic dSph companions, both And I and And II can be classified as second parameter objects. For the Galactic dSphs the second parameter nature of the HB morphology is, with the possible exception of Draco and Sculptor, established via main sequence turnoff photometry to result from significant populations of stars with intermediate ($\sim$1 – 10 Gyr) ages. Indeed, as inferred from the numbers and luminosities of these intermediate-age stars, the Galactic dSphs show a remarkable diversity in the star formation histories (e.g. recent reviews of Da Costa 1998 and Grebel 1999).

Our results for And I and And II indicate that this diversity of star formation histories applies also to the M31 dSph system. While both And I and And II are second parameter systems, and thus probably contain sizeable intermediate-age populations (albeit perhaps of different mean age) they differ considerably in detail. And II contains relatively more blue HB stars and RR Lyrae variables than And I (Sect. 3.1.1) indicating a higher fraction of older stars. Yet And II also has a relatively higher fraction of faint blue stars (Sect. 3.1.4) which conceivably represent the tip of the main sequence for a $\sim$2 Gyr old population. And II also has an identified population of upper-AGB (intermediate-age) stars (Sect. 3.5.2) which And I apparently lacks. Further, And II possesses a much broader internal abundance spread compared with And I (cf. Fig. 9) despite the similar mean abundances of these two galaxies. On the other hand, And I possesses a radial gradient in its HB morphology (cf. Paper I) which And II does not. Thus there seems little doubt that even on the basis of just these two objects, we can conclude that the diversity of star formation and chemical enrichment histories seen in the Galactic dSphs is also seen among the M31

dSphs. In that sense M31's and the Galaxy's dSph satellite systems are again similar.

Perhaps the only systematic difference that exists between these two sets of dSph galaxies is that the high luminosity markers of intermediate-age populations, namely upper-AGB carbon stars, appear to be relatively less frequent in the M31 dSph systems than in the Galactic dSph systems. Such stars are known in And II but aren't found in And I or And III (e.g. Armandroff 1994) and the published c-m diagrams for And V, And VI and And VII don't suggest the presence of many candidate upper-AGB stars in these systems either. A specific search for carbon stars is called for, particularly as regards the newly identified M31 dSphs. If, however, this difference in frequency of upper-AGB stars stands up to a more detailed and complete analysis, then it may indicate that there is an "environmental effect" governing the evolution of these galaxies, particularly as regards the fraction of the stellar populations with ages less than ∼5–6 Gyr. Such an environmental effect would be in the sense that conditions for retaining gas are less favorable for satellites of galaxies with massive, rapidly formed bulges (e.g. M31), than they are for the satellites of small bulge systems like the Milky Way. Such an effect is not inconsistent with the conclusions of van den Bergh (1994, see also Einasto *et al.* 1974) who noted that ram pressure stripping in gaseous coronae, supernova-driven galactic winds and a high UV flux from a parent galaxy could all affect the evolution of a satellite dwarf. The satellites most affected would be those which are less massive or less dense and which are on orbits that take them to smaller galactocentric distances (e.g. Hirashita *et al.* 1997).

One more point concerning the M31 and the Galactic dSph satellite systems can be made. As commented on by a number of authors (e.g. Armandroff *et al.* 1999, Grebel & Guhathakurta 1999), with the addition of the newly discovered objects to the list of M31 dSph companions, and now the confirmation here that And II is associated with M31 and not M33, it is apparent that the systems of dSph galaxies associated with M31 and the

Galaxy are roughly equivalent in size. For both galaxies the radius of the system of known dSph satellites is ∼250 kpc. The outermost members of these satellite systems are, of course, of prime importance in determining the mass and extent of the dark matter halos of the parent galaxies (cf. Zaritsky *et al.* 1989). With large ground-based telescopes it is now possible to measure line-of-sight velocities for the M31 dSph satellites and thus use these objects to provide further constraints on M31's mass. For example, Côté *et al.* (1999a) give a heliocentric velocity of –188 ± 3 km s^{-1} for And II from 9 measurements of 7 red giant members. Following Lynden-Bell (1999) this velocity corresponds to a line-of-sight velocity $V_\ell = +82$ km s^{-1} for And II in a frame in which M31 is at rest. Then, using $M \approx 3<V_\ell^2>R/G$ (cf. Lynden-Bell 1999) with our And II – M31 distance of ∼190 kpc (cf. Sect. 3.2), a mass estimate for M31 of 9×10^{11} $M_\odot$ results. While obviously additional objects are needed to improve the precision of this estimate, it is at least consistent with existing M31 mass determinations (e.g. 24×10^{11} $M_\odot$, Freeman 1999b and references therein). It is also consistent with the results of Zaritsky *et al.* (1993, see also Zaritsky & White 1994) who found masses of order 20×10^{11} $M_\odot$ within radii of ∼200 kpc from an ensemble analysis of satellite velocities for a set of isolated late-type spirals with luminosities similar to that of the Galaxy. Clearly line-of-sight velocities for the other M31 dSph companions are going to play a vital role in constraining the mass of M31's extended dark halo. In this context it is worth noting that the observed line-of-sight velocities for M31 satellites contain contributions from both the tangential and radial velocity components of the satellite. This contrasts with the situation for our Galaxy where the line-of-sight velocities for distant satellites are dominated by the radial component. Thus the M31 satellite velocities mass estimate will be less sensitive to assumptions regarding the distribution of orbital eccentricities than is the case for the Galaxy.

T. E. A. is grateful to Prof. Jeremy Mould, Director of the Research School of

Astronomy & Astrophysics, ANU, for support of a sabbatical visit during which some of the work reported here was carried out. The authors are also grateful to the NOAO WIYN Queue team, particularly Di Harmer and Paul Smith, for their efforts in obtaining the WIYN images used in this paper, and to Alistair Walker for supplying a copy of his NGC 1851 photometry. The comments of John Norris on a draft of this manuscript were also appreciated. This research was supported in part by NASA through grant number GO-06514 from the Space Telescope Science Institute, which is operated by AURA, Inc., under NASA contract NAS 5-26555.

REFERENCES

Aaronson, M., Gordon, G., Mould, J., Olszewski, E., & Suntzeff, N. 1985, ApJ, 296, L7

Armandroff, T. E. 1989, AJ, 97, 375

Armandroff, T. E. 1994, in An ESO/OHP Workshop on Dwarf Galaxies, eds G. Meylan & P. Prugniel, (Garching, ESO), p. 211

Armandroff, T. E., & Da Costa, G. S. 1999, in The Stellar Content of Local Group Galaxies, IAU Symposium 192, eds P. Whitelock & R. Cannon, (San Francisco, ASP), p. 203

Armandroff, T. E., Da Costa, G. S., Caldwell, N., & Seitzer, P. 1993, AJ, 106, 986

Armandroff, T. E., Davies, J. E., & Jacoby, G. H. 1998, AJ, 116, 2287

Armandroff, T. E., Jacoby, G. H., & Davies, J. E. 1999, AJ, 118, 1220

Azzopardi, M. 1994, in The Local Group: Comparative and Global Properties, eds A. Layden, R. C. Smith, & J. Storm, (Garching, ESO), p. 129

Baade, W., & Hubble, E. 1939, PASP, 51, 40

Beauchamp, D., Hardy, E., Suntzeff, N. B., & Zinn, R. 1995, AJ, 109, 1628

Bertelli, G., Bressan, A., Chiosi, C., Fagotto, F., & Nasi, E. 1994, A&AS, 106, 275

Buonanno, R., Corsi, C. E., Fusi Pecci, F., Hardy, E., & Zinn, R. 1985, A&A, 152, 65

Buonanno, R., Corsi, C. E., Zinn, R., Fusi Pecci, F., Hardy, E., & Suntzeff, N. B. 1998, ApJ, 501, L33

Burstein, D., & Heiles, C. 1982, AJ, 87, 1165

Caldwell, N. 1999, AJ, 118, 1230

Caldwell, N., Armandroff, T. E., Seitzer, P., & Da Costa, G. S. 1992, AJ, 103, 840

Caldwell, N., Armandroff, T. E., Da Costa, G. S., & Seitzer, P. 1998, AJ, 115, 535

Chaboyer, B., Demarque, P., & Sarajedini, A. 1996, ApJ, 459, 558

Côté, P., Mateo, M., Olszewski, E. W., & Cook, K. H. 1999a, ApJ, in press

Côté, P., Oke, J. B., & Cohen, J. G. 1999b, AJ, 118, 1645

Da Costa, G. S. 1998, in Stellar Astrophysics for the Local Group, eds A. Aparicio, A. Herrero, & F. Sánchez, (Cambridge, Cambridge Univ. Press), p. 351

Da Costa, G. S. 1999, in New Views of the Magellanic Clouds, IAU Symposium 190, eds Y.-H. Chu, N. B. Suntzeff, J. E. Hesser & D. Bohlender, (San Francisco, ASP), in press

Da Costa, G. S., & Armandroff, T. E. 1990, AJ, 100, 162

Da Costa, G. S., Armandroff, T. E., Caldwell, N., & Seitzer, P. 1996, AJ, 112, 2576 (Paper I)

Dekel, A., & Silk, J. 1986 ApJ, 303, 39

Einasto, J., Saar, E., Kaasik, A., & Chernin, A. D. 1974, Nature, 252, 111

Freeman, K. C. 1999a, in The Third Stromlo Symposium: The Galactic Halo, ASP Conf. Ser. 165, eds B. K. Gibson, T. S. Axelrod, & M. E. Putman, (San Francisco, ASP), p. 167

Freeman, K. C. 1999b, in The Stellar Content of Local Group Galaxies, IAU Symposium 192, eds P. Whitelock & R. Cannon, (San Francisco, ASP), p. 383

Frogel, J. A., & Elias, J. H. 1988, ApJ, 324, 823

Fusi Pecci, F., Buonanno, R., Cacciari, C., Corsi, C. E., Djorgovski, S. G., Federici, L., Ferraro, F. R., Parmeggiani, G., & Rich, R. M. 1996, AJ, 112, 1461

Gallart, C., *et al.* 1999a, ApJ, 514, 665

Gallart, C., Freedman, W. L., Aparicio, A., Bertelli, G., & Chiosi, C. 1999b, AJ, in press (astro-ph/9906121)

Grebel, E. K. 1999, in The Stellar Content of Local Group Galaxies, IAU Symposium 192, eds P. Whitelock & R. Cannon, (San Francisco, ASP), p. 17

Grebel, E. K. & Guhathakurta, P. 1999, ApJ, 511, L101

Green, E. M., & Norris, J. E. 1990, ApJ, 353, L17

Grillmair, C. J., *et al.* 1998, AJ, 115, 144

Guarnieri, M. D., Renzini, A., & Ortolani, S. 1997, ApJ, 477, L21

Harris, W. E. 1982, ApJS, 50, 573

Hartwick, F. D. A. 1976, ApJ, 209, 418

Hirashita, H., Kamaya, H., & Mineshige, S. 1997, MNRAS, 290, L33

Holtzman, J., *et al.* , 1995a, PASP, 107, 156

Holtzman, J. A., Burrows, C. J., Casertano, S., Hester, J. J., Trauger, J. T., Watson, A. M., & Worthey, G. 1995b, PASP, 107, 1065 (H95)

Hurley-Keller, D., Mateo, M., & Grebel, E. 1999, ApJ, 523, L25

Karachentsev, I. D. & Karachentseva, V. E. 1999, A&A, 341, 355

König, C. H. B., Nemec, J. M., Mould, J. R., & Fahlman, G. G. 1993, AJ, 106, 1819

Larson, R. B. 1974, MNRAS, 166, 585

Lee, M. G., Freedman, W. L., & Madore, B. F. 1993, ApJ, 417, 553

Lee, S.-W. 1977a, A&AS, 27, 381

Lee, S.-W. 1977b, A&AS, 29, 1

Lee, Y.-W., Demarque, P., & Zinn, R. 1994, ApJ, 423, 248

Lynden-Bell, D. 1999, in The Stellar Content of Local Group Galaxies, IAU Symposium 192, eds P. Whitelock & R. Cannon, (San Francisco, ASP), p. 39

Mac Low, M.-M., & Ferrara, A. 1999, ApJ, 513, 142

Majewski, S. R., Siegel, M. H., Patterson, R. J., & Rood, R. T. 1999, ApJ, 520, L33

Mateo, M. 1998, ARA&A, 36, 435

Mighell, K. J., & Rich, R. M. 1996, AJ, 111, 777

Mould, J., & Kristian, J. 1990, ApJ, 354, 438

Norris, J. E., Freeman, K. C., & Mighell, K. J. 1996, ApJ, 462, 241

Olszewski, E. W., Pryor, C., & Armandroff, T. E. 1996, AJ, 111, 750

Ratnatunga, K. U., & Bahcall, J. N. 1985, ApJS, 59, 63

Schlegel, D. J., Finkbeiner, D. P., & Davis, M. 1998, ApJ, 500, 525

Shapley, H. 1938, Harvard College Obs. Bull., No. 908, 1

Smecker-Hane, T. A., Mandushev, G. I., Hesser, J. E., Stetson, P. B., Da Costa, G. S., & Hatzidimitriou, D. 1999, in Spectrophotometric Dating of Stars and Galaxies, ASP. Conf. Ser., eds I. Hubeny, S. Heap & R. Cornett, (San Francisco, ASP), in press

Stetson, P. B., 1998, PASP, 110, 1448

Stetson, P. B., Bolte, M., Harris, W. E., Hesser, J. E., van den Bergh, S., VandenBerg, D. A., Bell, R. A., Johnson, J. A., Bond, H. E., Fullton, L. K., Fahlman, G. G., & Richer, H. B. 1999, AJ, 117, 247

Stetson, P. B., Hesser, J. E., & Smecker-Hane, T. A. 1998, PASP, 110, 533

Tinsley, B. M. 1980, Fundamentals of Cosmic Physics, 5, 287

Vader, J. P. 1986, ApJ, 305, 669

Vader, J. P. 1987, ApJ, 317, 128

van den Bergh, S. 1994, ApJ, 428, 617

Walker, A. R. 1992, PASP, 104, 1063

Walker, A. R. 1994, PASP, 106, 828

Whitmore, B., & Heyer, I. 1997, Instrument Science Report WFPC2 97-08 (Baltimore: STScI) (WH97)

Zaritsky, D., Olszewski, E. W., Schommer, R. A., Peterson, R. C., & Aaronson, M. 1989, ApJ, 345, 759

Zaritsky, D., Smith, R., Frenk, C., & White, S. D. M. 1993, ApJ, 405, 464

Zaritsky, D., & White, S. D. M. 1994, ApJ, 435, 599

Zinn, R. 1978, ApJ, 225, 790

Zinn, R., & West, M. J. 1984, ApJS, 55, 45

A. A Revised Analysis of the Andromeda I Data

In Paper I we analyzed our HST/WFPC2 photometry of Andromeda I using the 0.04 mag/800 pixel ramp correction for CTE effects, the Holtzman *et al.* (1995b) zeropoints for the $F555W$ to V and $F450W$ to B transformations, and the Burstein & Heiles (1982) reddening estimate. All three of these processes or assumptions, however, have been superseded by new techniques or new data. Thus, to allow a proper comparison of Andromeda I with the Andromeda II results presented in this paper, we have reanalyzed the And I photometry in a manner analogous to that used for And II. In particular, we have applied the WH97 CTE correction formalism, as described in Sect. 2.1.1, to the original And I aperture photometry measurements. We have also used the adjusted $B-V$ zeropoint discussed in Sect. 2.1.3 and restricted the data to just that for the WF CCDs. The resulting And I c-m diagram is shown in Fig. 13. Note that candidate variable stars in And I have not been excluded from this c-m diagram (cf. Fig. 5).

The majority of the And I results presented in Paper I are not changed by this reanalysis. In particular, the horizontal branch morphology, the horizontal branch morphology gradient, and the inferences drawn concerning the age of the bulk of the stellar population in And I remain unaffected by the small changes in the photometric data. There are, however, some minor modifications which we outline here. First, in the revised photometry, the mean magnitude of the horizontal branch is slightly brighter than the value presented in Paper I ($V(\mathrm{HB}) = 25.23 \pm 0.04$ rather than 25.25 ± 0.04). Further, the Schlegel *et al.* (1998) reddening maps predict $\mathrm{E}(B-V) = 0.053$ for And I; we adopt $\mathrm{E}(B-V) = 0.05 \pm 0.01$ and $\mathrm{A}_V = 0.17 \pm 0.03$ mag. These values are slightly higher than those adopted in Paper I. Consequently, for our And I mean abundance of <[Fe/H]> = –1.46 ± 0.12 (see following paragraph) and our adopted distance scale, the line-of-sight distance to And I is marginally smaller than the value given in Paper I. We find $(\mathrm{m–M})_0$

= 24.49 ± 0.06 corresponding to a distance of 790 ± 25 kpc. The difference between the Paper I value (810 ± 30 kpc) and the new distance is sufficiently small, however, that the relative line-of-sight distance between M31 and And I given in Paper I, 0 ± 70 kpc, is essentially unaltered. This is also the case for the true distance of And I from the center of M31 – it lies between ∼45 and ∼85 kpc, as discussed in Paper I.

As regards the mean metallicity of And I, applying the method of analysis described in Sect. 3.3 to the revised photometry yields a mean abundance of <[Fe/H]> = –1.46 ± 0.12 from six 0.2 V mag wide bins on the upper giant branch and <[Fe/H]> = –1.20 ± 0.25 from two similar bins on the lower giant branch. Here the uncertainty given for each abundance includes the statistical error in the mean colors, the effects of a $(B-V)$ zeropoint uncertainty of ±0.03 mag and a distance modulus uncertainty of ±0.06 mag, and the effect of uncertainty in the abundance calibration derived from the standard globular cluster giant branches. As for And II no one uncertainty dominates the total error for the upper giant branch value, while for the lower giant branch, the $(B-V)$ zeropoint uncertainty is the major contributor to the abundance error. It is worth noting that these abundance estimates have been derived without applying any additional color shift to the globular cluster standard giant branches, as was found necessary in Paper I. A comparison of the standard globular giant branches with the new And I photometry for an apparent distance modulus of $(m–M)_V = 24.66$ and a reddening $E(B-V) = 0.05$ mag is also shown in Fig. 13. This figure also shows the mean giant branch colors for the adopted 0.2 V mag wide bins (cf. Fig. 8).

Because of the additional uncertainty in the lower giant branch mean colors caused by contamination from (relatively metal-rich) M31 field giants, and for the reasons discussed in Sect. 3.3 above, we regard the And I mean abundance derived from the upper giant branch as the more reliable determination. Surprisingly, despite the reanalysis carried out

here, this mean abundance, <[Fe/H]> = –1.46 ± 0.12, has turned out to be very similar to the value preferred in Paper I <[Fe/H]> = –1.45 ± 0.2). This is also true of the intrinsic abundance spread in And I. Applying the analysis technique described in Sect. 3.4 to the revised And I photometry results in σ_{int}([Fe/H]) ≈ 0.21 dex, an inter-quartile range of 0.36 dex and a central two-thirds of the sample range of 0.49 dex. The corresponding values in Paper I were 0.20, 0.30 and 0.45 dex, respectively. The And I abundance distribution from the 117 stars with $22.5 \leq V \leq 23.5$ is shown as the dashed line in Fig. 9. This distribution is clearly narrower than that of And II and is approximately gaussian in shape.

Fig. 1.— The location of the section of And II imaged with WFPC2 is shown superposed on a ground-based image of this dSph obtained with the WIYN telescope. The WIYN image is the combination of three 400 s exposures in the V band and has images with FWHM $\approx$ 0.55″. North is at the top and East is to the left.

Fig. 2.— A mosaic of the And II WFPC2 field made from the combination of four 1200 s $F555W$ exposures. North is indicated by the direction of the arrow and East by the line. Both indicators are 10″ in length. The center of And II lies near the WF3/WF4 overlap region close to the edge of the frame. The majority of WF2 then lies beyond And II's core radius. This positioning was necessary to avoid bright foreground stars.

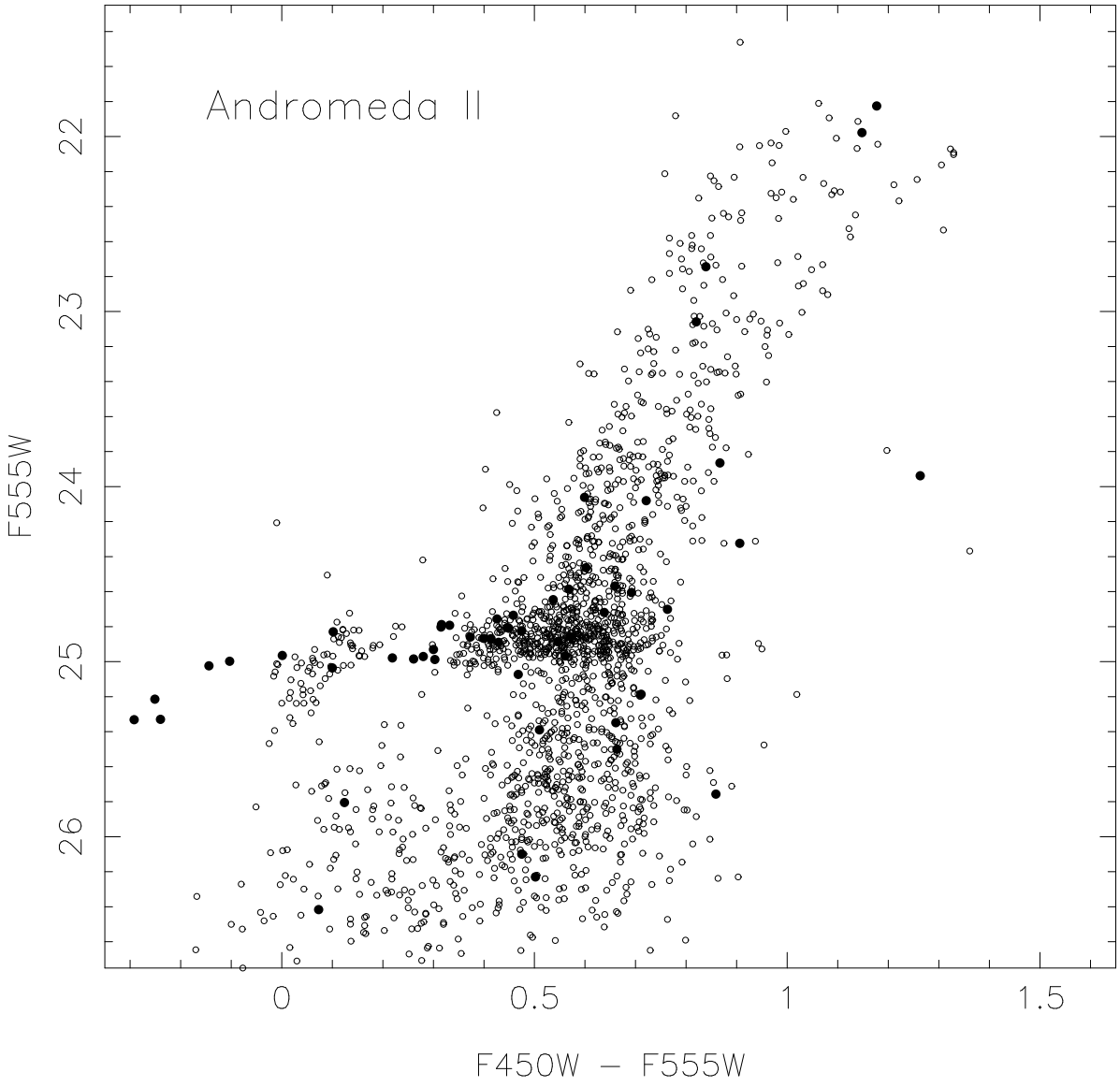

Fig. 3.— The combined Andromeda II color-magnitude diagram on the WFPC2 system of Holtzman *et al.* (1995b) after the application of the Whitmore & Heyer (1997) CTE corrections. Stars from all three WF CCDs are plotted. The filled symbols are stars which show large differences between the two sets of observations. The majority of these stars are likely to be And II variables.

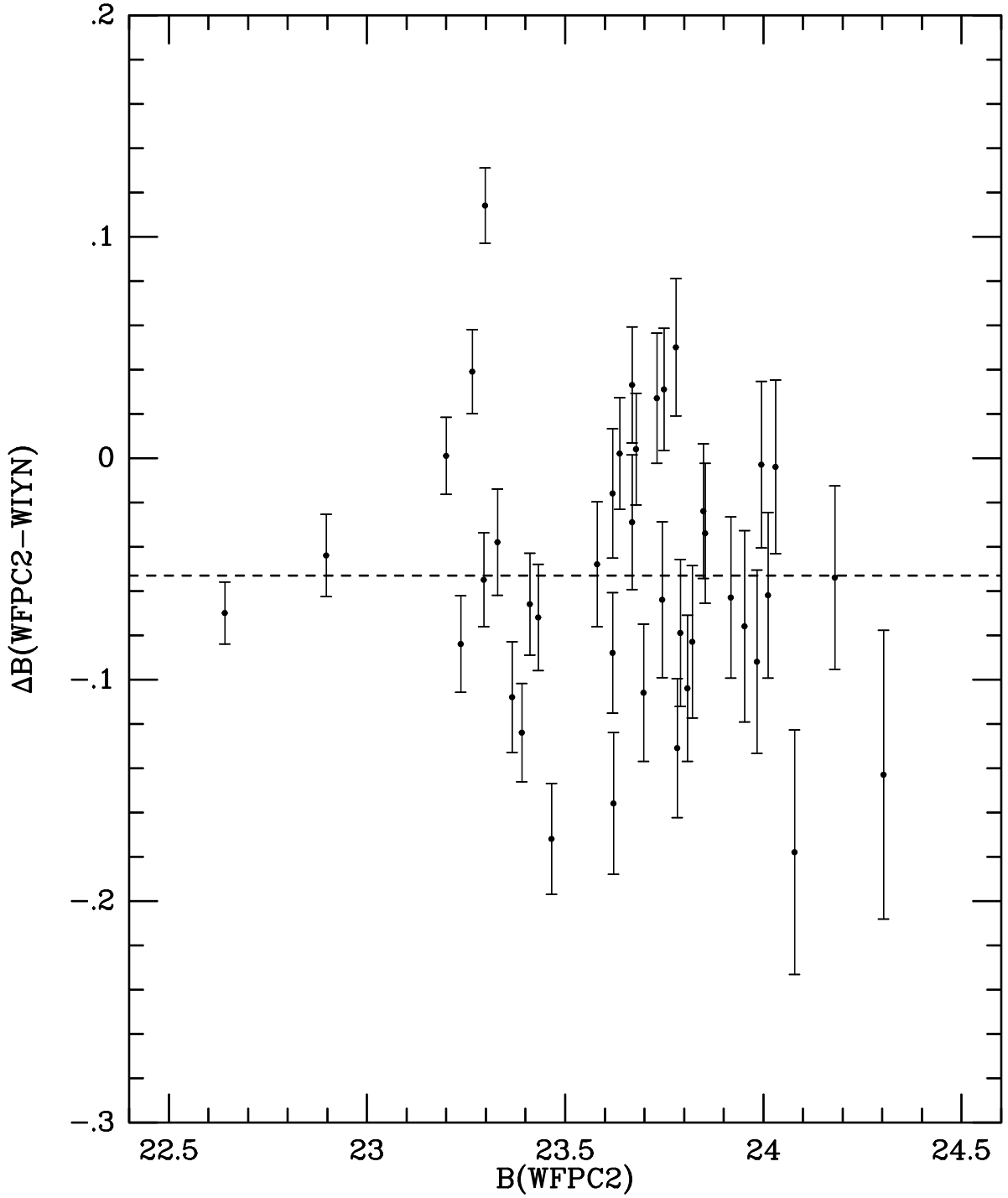

Fig. 4.— A plot of the difference between B_{WFPC2}, derived from the $F450W$ photometry via application of the transformations in Holtzman *et al.* (1995b), and B_{WIYN}, derived from ground-based imaging, against B_{WFPC2} for And II red giants. The mean offset is –0.053 ± 0.010 mag.

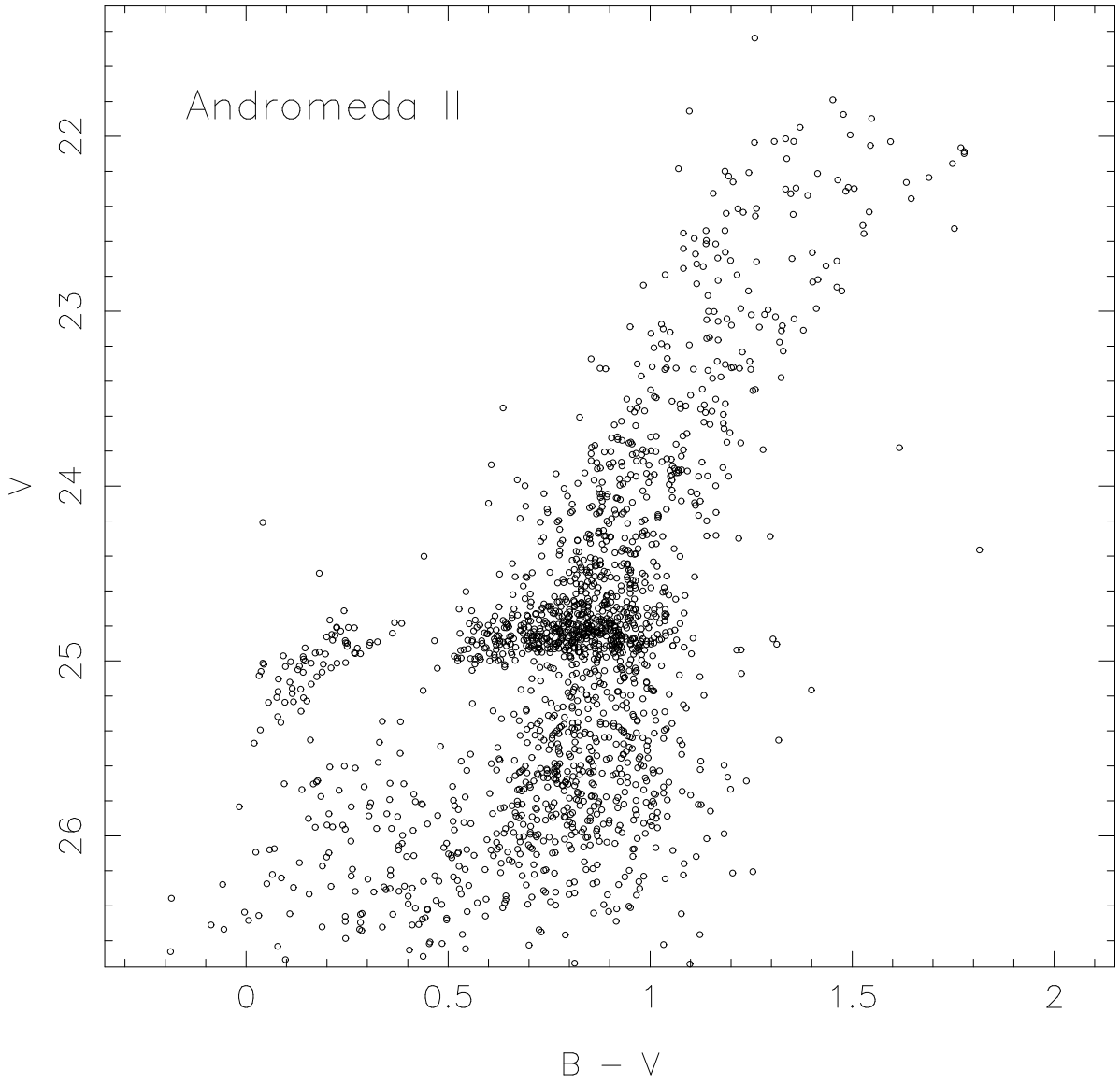

Fig. 5.— The combined Andromeda II color-magnitude diagram on the standard B,V system. The $B - V$ zeropoint has been shifted redwards by 0.055 mag relative to the transformation of Holtzman *et al.* (1995b), in accordance with our ground-based determination of the zeropoint (see Sect. 2.1.3). Candidate variables (cf. Fig. 3) have been excluded from this plot.

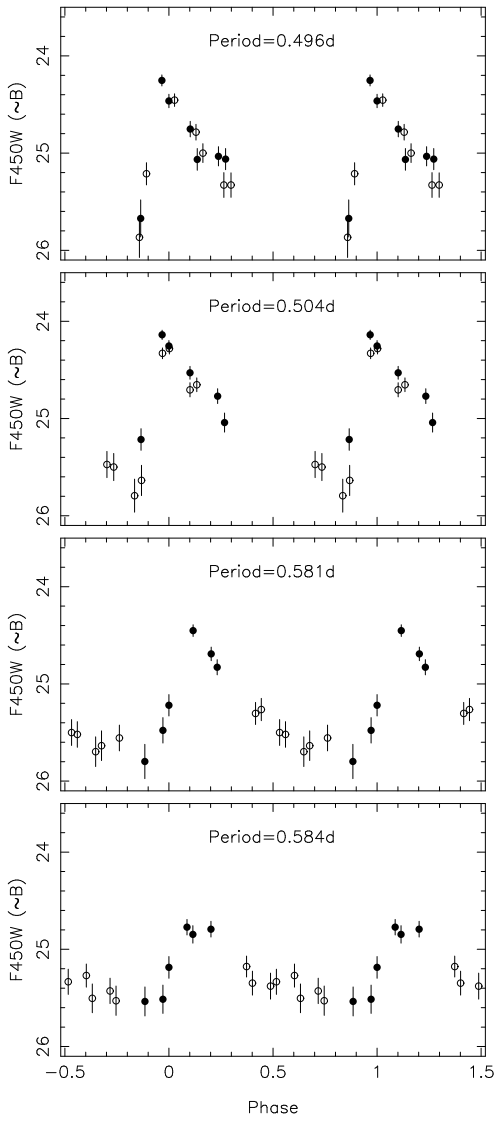

Fig. 6.— $F450W$ light curves for 4 And II RR Lyrae stars. These stars come from the sample of candidate variables identified in Fig. 3. Two cycles are plotted for each variable with open and closed symbols representing the two sets of observations. The error bars are those from the photon statistics. The adopted periods are given in each panel.

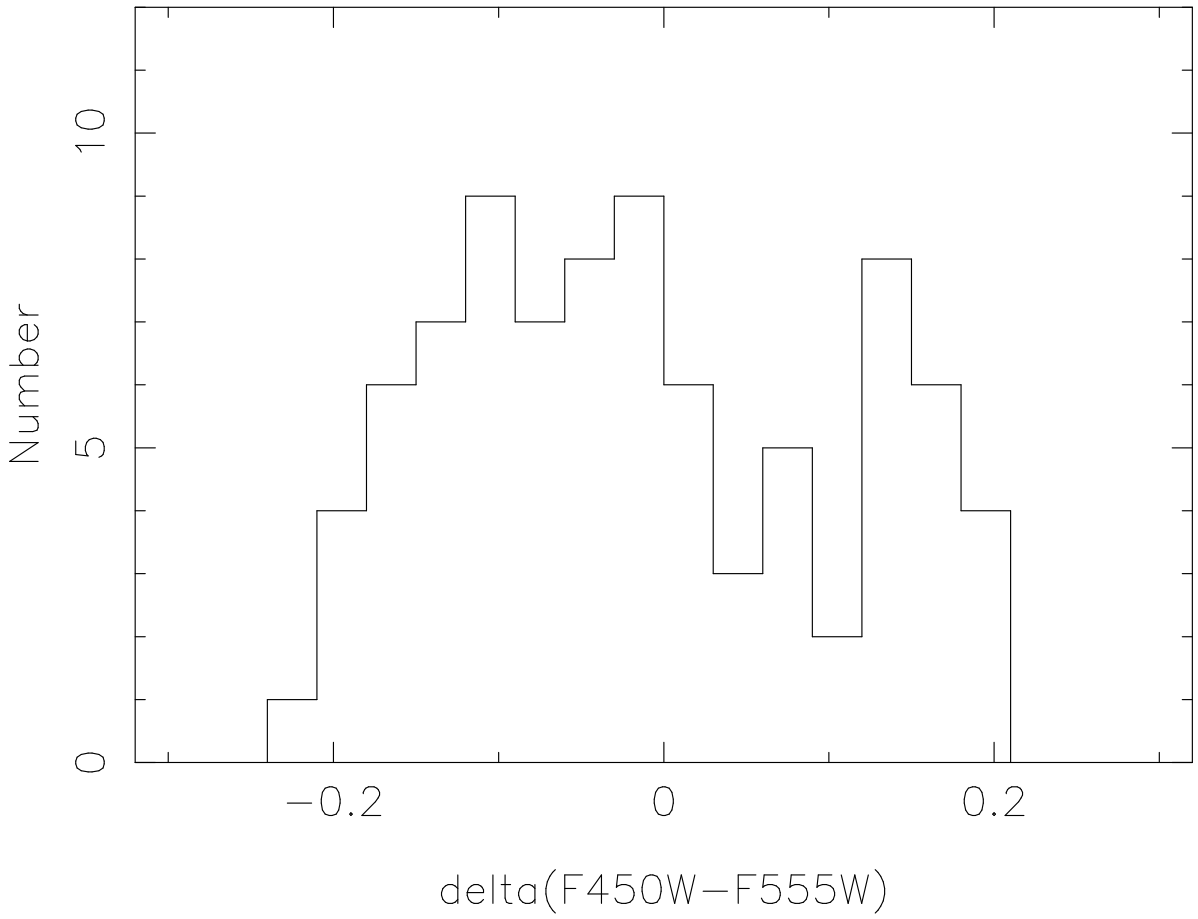

Fig. 7.— Histogram of $F450W - F555W$ residuals from the mean And II giant branch for 85 stars with $22.2 \leq F555W \leq 23.2$. The photometric errors for stars in this magnitude range is $\sigma_{err}(F450W - F555W) \approx 0.02$ mag. The bin size is 0.03 mag.

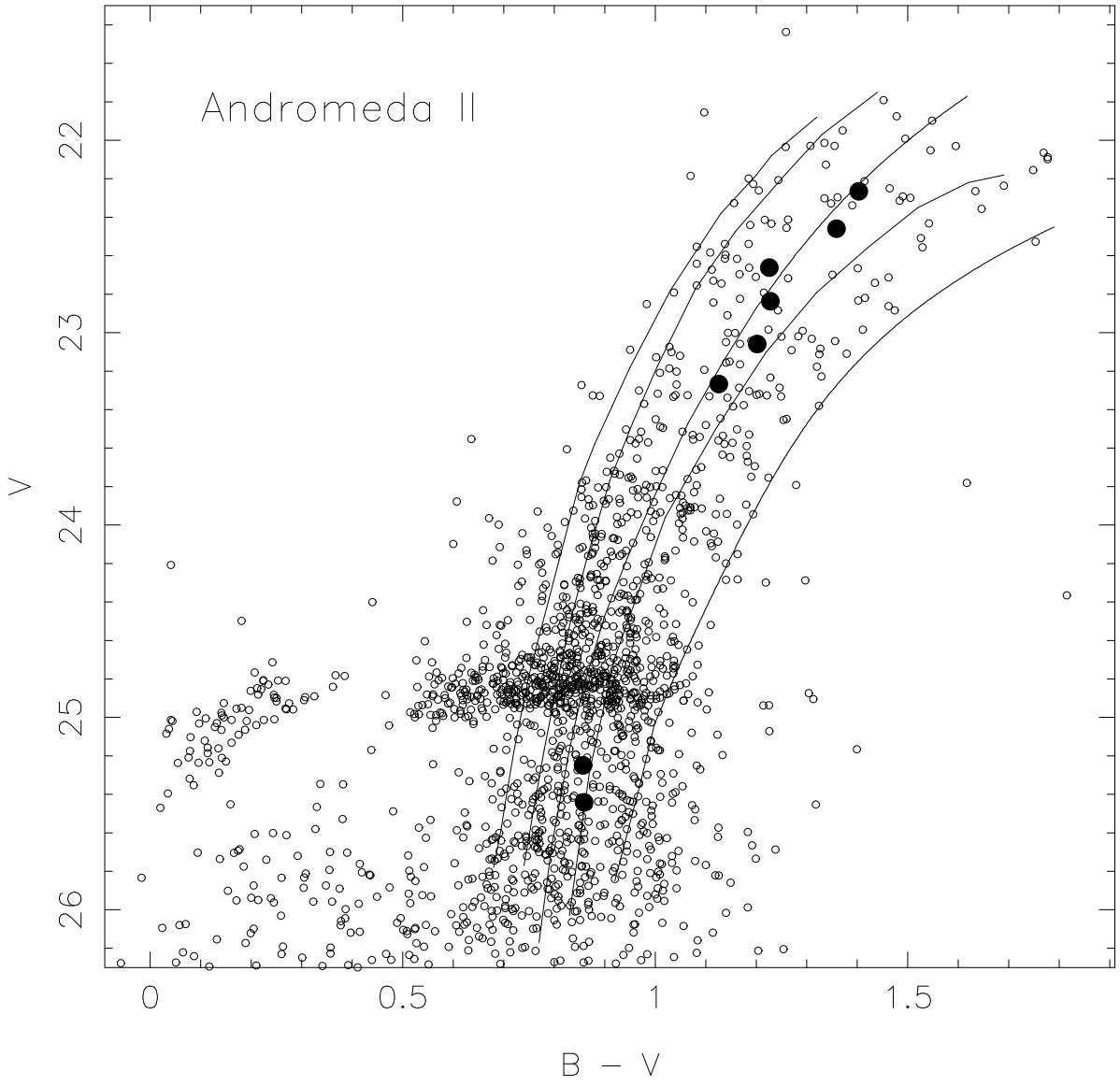

Fig. 8.— The Andromeda II (V, $B-V$) color-magnitude from Fig. 5 is shown superposed with the giant branches of the standard globular clusters M68 ([Fe/H]=–2.09), M55 ([Fe/H]=–1.82), NGC 6752 ([Fe/H]=–1.54), NGC 362 ([Fe/H]=–1.28) and 47 Tuc ([Fe/H]=–0.71). An And II apparent distance modulus of $(m - M)_V = 24.36$ and a reddening of $E(B-V) = 0.06$ have been used to place the globular cluster giant branch data on this diagram. The filled symbols give the mean And II giant branch colors for ± 0.1 V mag bins.

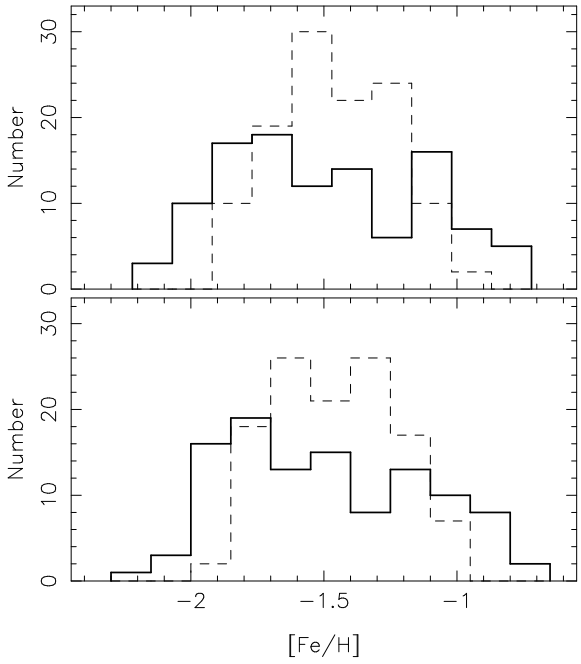

Fig. 9.— A comparison of the abundance distributions for the dSphs And I (dashed line) and And II (solid line). These abundance distributions have been derived in an identical manner from similar WFPC2 data. The And I sample contains 117 red giants while that for And II contains 108 stars. The bin width is 0.15 dex. The two panels show the effect of offsetting the origin of the histogram bins by 0.07 dex.

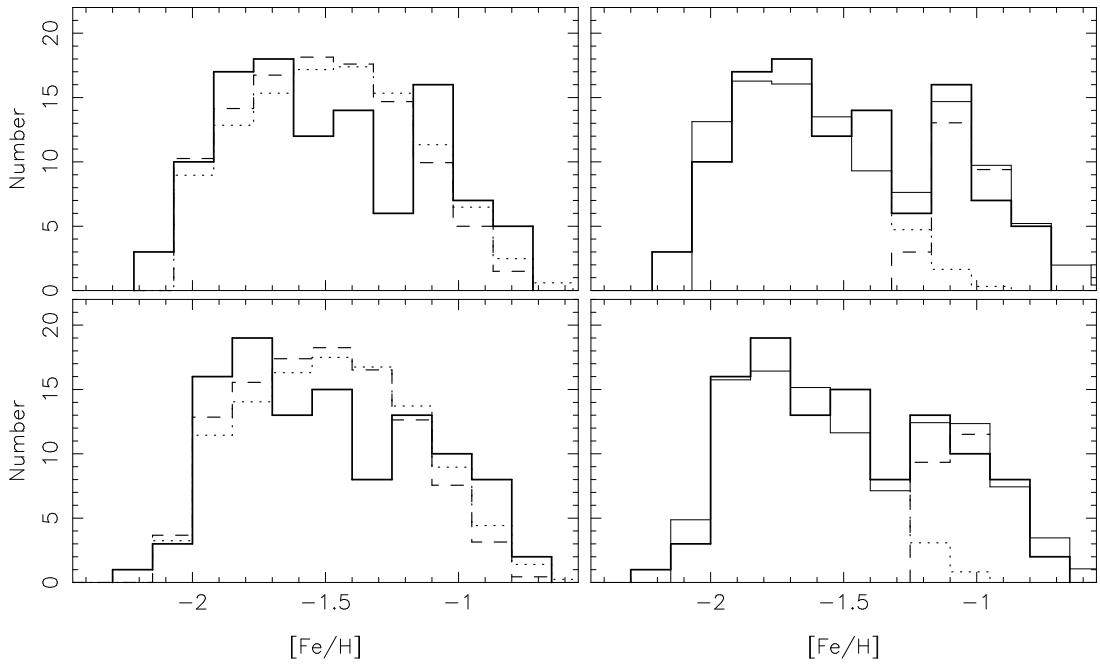

Fig. 10.— The abundance distribution in And II compared to simple chemical enrichment models. In all panels the thick solid line is the observed distribution inferred from the colors of the 108 red giants with $22.15 \leq V \leq 23.35$. The bin width is 0.15 dex. The upper and lower panels show the histograms that result from offsetting the origin of the bins by 0.07 dex. The left panels also show the predictions of one component "steady gas loss" (dotted line) and "sudden gas loss" (dashed line) models. The right panels show the predictions of a two component steady gas loss model. Here the thin solid line is the sum of the two components. The dotted and the dashed lines show the contributions of the individual components in the region where they overlap. See Sect. 3.4 for details of the parameters for this model.

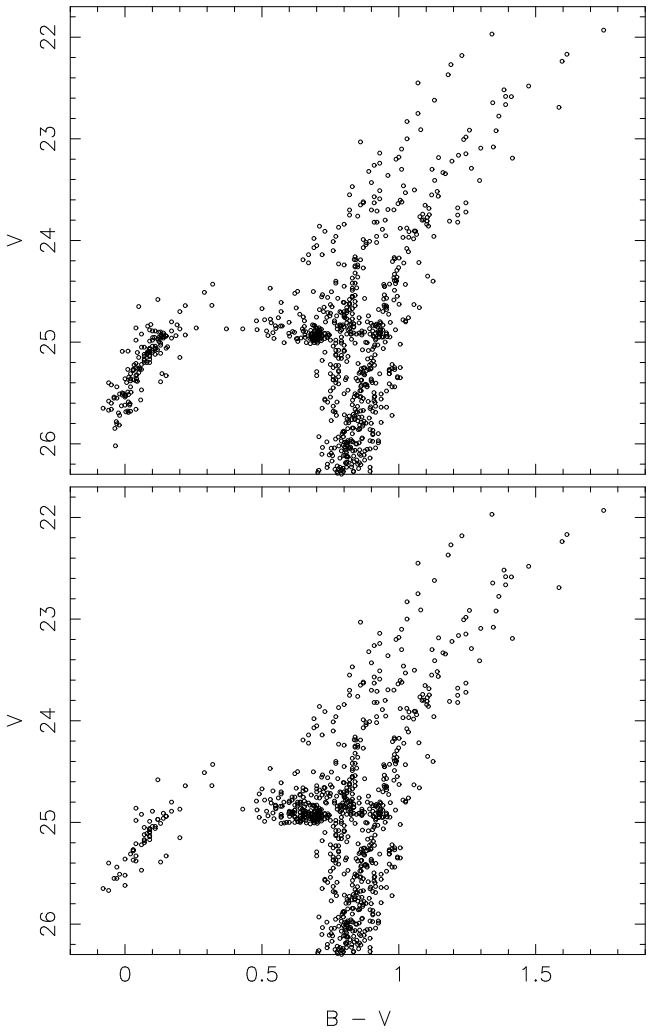

Fig. 11.— The upper panel is a composite c-m diagram made up from observed c-m diagrams for the Galactic globular clusters M55 ([Fe/H] = –1.82), NGC 1851 ([Fe/H] = –1.29) and 47 Tuc ([Fe/H] = -0.71), with the relative star numbers (44:45:11) scaled to reflect the And II abundance distribution. This c-m diagram clearly has relatively more blue horizontal branch (HB) stars than does And II (cf. Fig. 5). In the lower panel all the NGC 1851 blue HB and 40% of the M55 blue HB stars have been replaced with red HB stars from NGC 362 (∼80%) and 47 Tuc (∼20%). The horizontal branch morphology of this c-m diagram is now a better match to that of And II.

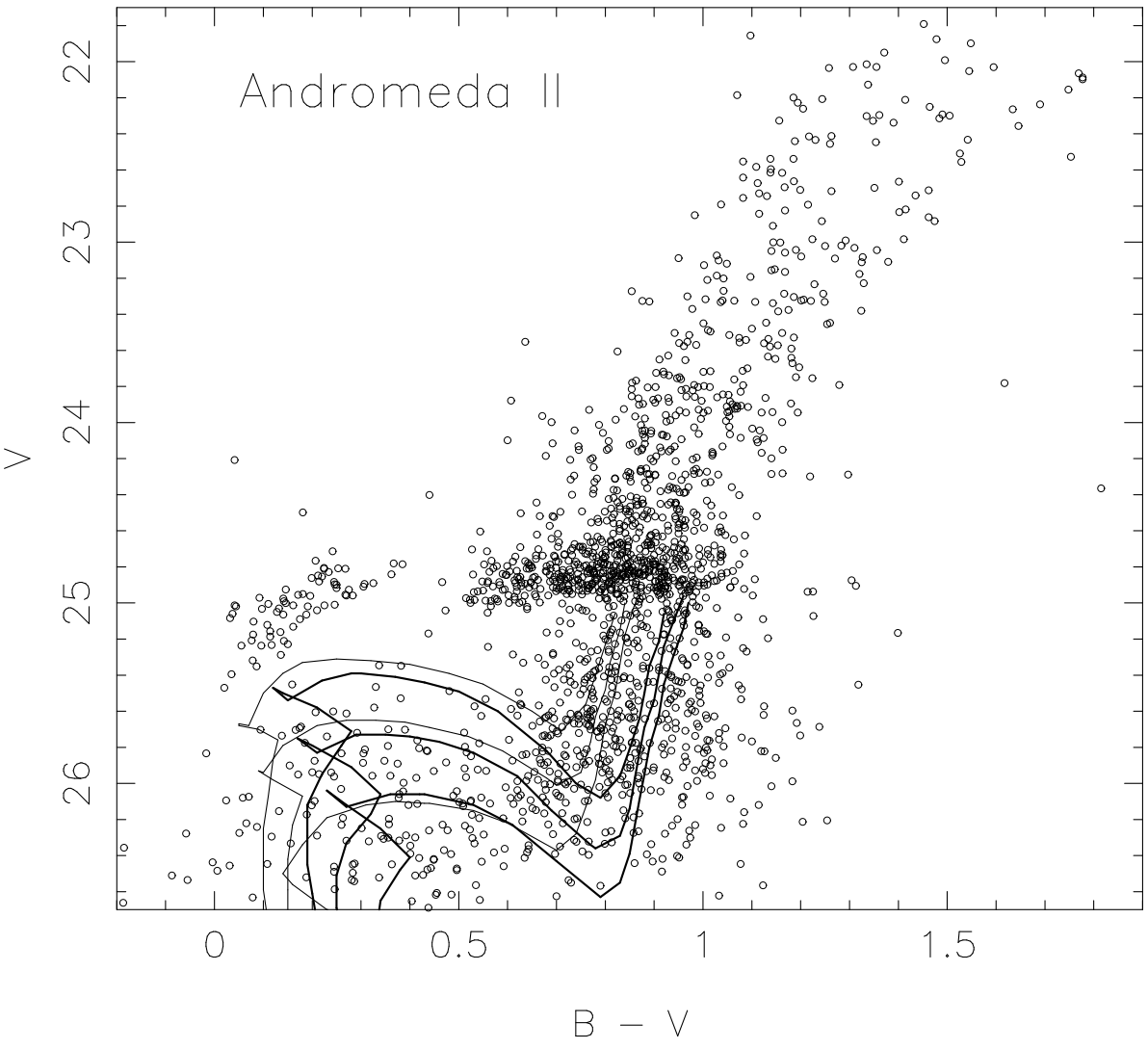

Fig. 12.— A comparison of the And II "faint blue stars" with theoretical isochrones from Bertelli *et al.* (1994). The thick lines are for an abundance $\log(z/z_{sun}) = -0.7$ and ages of 1.25, 1.6 and 2 Gyr. The thin lines are for $\log(z/z_{sun}) = -1.3$ and ages of 1.6, 2 and 2.5 Gyr. Note that the data are seriously incomplete for $V \gtrsim 26.0$ and $B \gtrsim 26.7$ mag.

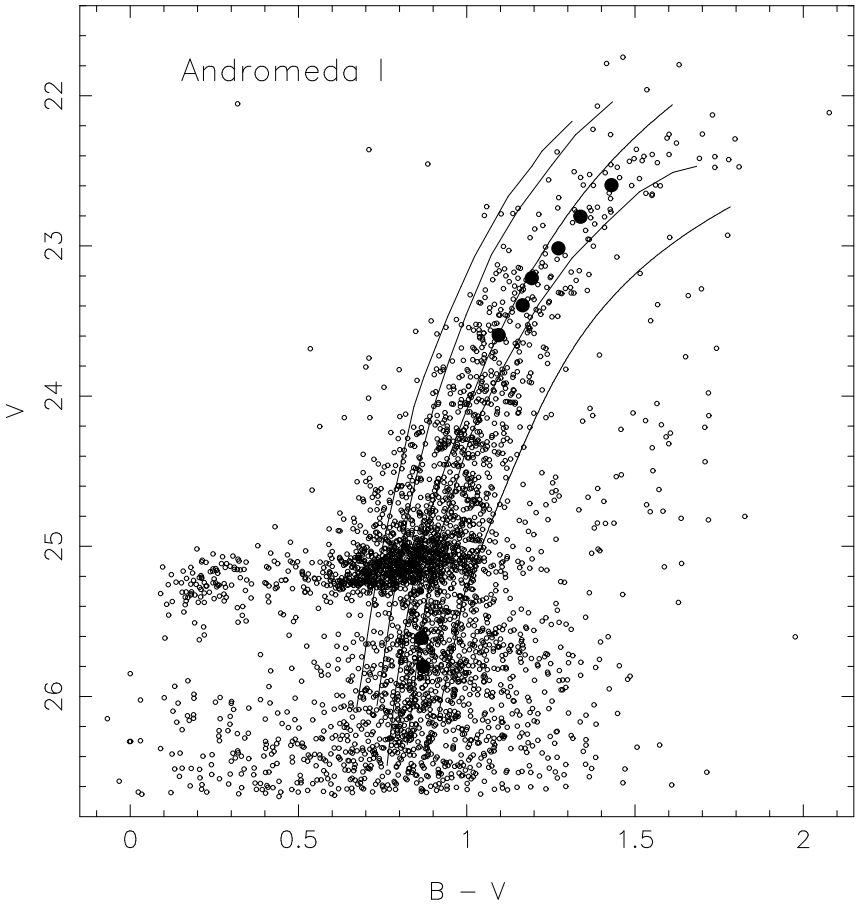

Fig. 13.— A color-magnitude diagram for Andromeda I based on a reanalysis of the photometry presented in Paper I. The data shown are for the three WF CCDs and no attempt has been made to exclude any candidate variables. The $B-V$ zeropoint has been shifted redwards by 0.055 mag relative to the transformation of Holtzman *et al.* (1995b), in accordance with the discussion in Sect. 2.1.3. Shown superposed on the revised photometry are the giant branches of the standard globular clusters M68 ([Fe/H]=–2.09), M55 ([Fe/H]=–1.82), NGC 6752 ([Fe/H]=–1.54), NGC 362 ([Fe/H]=–1.28) and 47 Tuc ([Fe/H]=–0.71). An And I apparent distance modulus of $(\mathrm{m}-\mathrm{M})_V = 24.66$ and a reddening of $\mathrm{E}(B-V) = 0.05$ have been used to place the globular cluster giant branch data in this diagram. The filled symbols give the mean And I giant branch colors for ± 0.1 V mag bins.

Table 1. Photometric Errors.

F555W	Mean Error in F555W	Mean Error in F450W–F555W	F450W	Mean Error in F450W
21.5–23.0	0.012	0.014	22.0–24.4	0.017
23.0–24.0	0.014	0.022	24.4–24.9	0.023
24.0–24.5	0.019	0.033	24.9–25.4	0.036
24.5–25.0	0.032	0.046	25.4–25.8	0.044
25.0–25.4	0.038	0.066	25.8–26.2	0.065
25.4–25.8	0.050	0.077	26.2–26.6	0.086
25.8–26.1	0.068	0.108	26.6–26.9	0.122
26.1–26.4	0.077	0.136	26.9–27.2	0.151

This figure "fig1.jpg" is available in "jpg" format from:

http://arXiv.org/ps/astro-ph/9911020v1

This figure "fig2.jpg" is available in "jpg" format from:

http://arXiv.org/ps/astro-ph/9911020v1